FROM EXTINCTION TO RECOVERY: LATE TRIASSIC AND EARLY-MIDDLE JURASSIC AMMONOID MORPHOLOGY

By

JIN ZHANG
B.Sc., Nanjing University, Nanjing, China, 1982
M.Sc., Nanjing Institute of Geology and Palaeontology, Academia Sinica, Nanjing, China, 1988

A THESIS SUBMITTED IN PARTIAL FULFILMENT OF
THE REQUIREMENTS FOR THE DEGREE OF
MASTER OF SCIENCE

in

THE FACULTY OF GRADUATE STUDIES
DEPARTMENT OF EARTH AND OCEAN SCIENCES

We accept this thesis as conforming to the required standard

THE UNIVERSITY OF BRITISH COLUMBIA

OCTOBER 2002

In presenting this thesis in partial fulfilment of the requirements for an advanced degree at the University of British Columbia, I agree that the Library shall make it freely available for reference and study. I further agree that permission for extensive copying of this thesis for scholarly purposes may be granted by the head of my department or by his or her representatives. It is understood that copying or publication of this thesis for financial gain shall not be allowed without my written permission.

Department of Earth and Ocean Sciences

The University of British Columbia
Vancouver, Canada

Date May 01/2003

DE-6 (2/88)

Abstract

As one of the five largest mass extinctions occurring in the Phanerozoic, the extinction at the end of the Triassic dramatically affected the evolution of ammonoids, taxonomically and morphologically. The major aim of this thesis is to compare and contrast the ammonoid morphological evolution for the Upper Triassic Carnian Stage through the Middle Jurassic Bajocian Stage and explore the relationships among ammonoid morphospace, ornamentation, and suture types.

"Buckman's law of covariation" (Westermann, 1966) indicates that, in the Bajocian, certain combinations of ammonoid morphological parameters occur more frequently and presumably conferred an evolutionary advantage. In brief, the law states that ammonoid whorl width, umbilical ratio, and strength of ornamentation are negatively correlated with whorl expansion rate. However, since "Buckman's law of covariation" was established for a group of Middle Jurassic Hildoceratids, a major question being addressed in this thesis is whether the "Buckman's law of covariation"' is more widely applicable to Upper Triassic and Lower-Middle Jurassic ammonoid data.

Specimens were sampled at genus level. Data are mainly taken from AMMON database and other published literature. Raup's (1966) numerical model is used in this thesis to describe the basic shell geometry of planispiral ammonoids. The density of the occurrence of real shell geometries (whorl expansion W, and umbilical ratio U) for a set of ammonoid samples was contoured to create a density-contour map and three-dimensional surface plot for each stage. The results prove that "Buckman's law of covariation" is apparently applicable to Jurassic ammonoids, but weakly to Late Triassic ammonoids. Combining the appearance and the morphology of heteromorph ammonoids,

three intervals can be recognized: 1. Late Triassic (pre-extinction interval), 2. Early Jurassic (post-extinction interval), and 3. Middle Jurassic (recovery interval).

The possible covariations between whorl shape WWWH (ratio of whorl width WW and whorl height WH) and the basic morphological features W and U are approached in this thesis because this is important part in "Buckman's law of covariation". The U-WWWH contoured density maps and the W-WWWH contoured density maps indicate positive correlations between U and WWWH, and negative correlations between W and WWWH. In consideration of taxonomic effects, I also explore these relationships by using taxonomic subsets (for the superfamilies Nathorstitaceae and Tropitaceae) of the Norian Stage. The positive correlations between U and WWWH and negative correlations between W and WWWH can also be seen.

W-U density contoured maps of equidimensionally whorl shaped ammonoids (WWWH $\approx$ 1) are created for Upper Triassic (Carnian) through the Middle Jurassic (Bajocian) in order to explore whether ammonoids adopt shell shapes with maximal hydrodynamic efficiency. Low drag coefficient (C_D) values determined from the data of shell models (Chamberlain, 1980) are plotted on these maps. Generally Later Triassic and Middle Jurassic ammonoids have broad distribution across W-U morphospace and relatively low hydrodynamic efficiency. Early Jurassic ammonoids have better hydrodynamic efficiency and linear W-U geometric patterns. Areas of high drag on the uncoiled side of the offlap line (W = 1/D) are only exploited in the Norian and Bajocian due to the existence of heteromorph ammonoids in these two stages.

The accumulated morphological range diversity index (MRDI), which describes the range of the morphospace occupied, is used to study morphological changes through

the stages. There are two declines in the MRDI: from the Norian to the Hettangian and from the Toarcian to the Aalenian.

In this thesis, I explore the possible correlation between Late Triassic ammonoid shell geometry and suture type. In the Upper Triassic there are three types of suture and the shell geometries are quite diverse, while in the Hettangian Stage, there is only one type of suture and the shell geometry spectrum is greatly reduced. The research shows that involute Upper Triassic shells tend to have complex sutures, whereas evolute shells have simple sutures. Hettangian ammonoids are relatively evolute but their sutures are complex. Reasons for these differences are not yet clear.

TABLE OF CONTENTS

Acknowledgments

I express my special thanks to my advisor, Dr. Paul L. Smith, for his guidance, encouragement, patience, and financial support. This valuable help made it possible for me to complete my thesis. His guidance throughout my years at UBC has benefited me a great deal, not only academically, but also personally. In addition, his wonderful sense of humour has made my study at UBC always joyful.

Special thanks are due to Dr. H. W. Tipper (Geological Survey of Canada) whose encouragement and suggestions have improved the manuscript. The other members of my committee, Dr. Kurt Grimm (UBC) and Dr. Stuart Sutherland (UBC) gave their valuable comments in committee meetings and read drafts of the manuscript, which improved the final product.

I owe a great deal to Dr. Bo Liang (ALI technologies Inc., Richmond), a former graduate student at EOS of UBC, who kindly provided his useful suggestions and advice, especially in computer application and statistical methods. I benefited greatly from Bo Liang's help. My many thanks go to Dr. Jiuping Chen, a post-doctoral fellow in EOS, UBC, who provided his kind help in creation of a data griding program.

I sincerely thank Ms. Reyna Brown (a research assistant in UBC Paleontology and Jurassic Stratigraphy Laboratory). She helped me in data acquisition, data input, and reading of the early drafts of the thesis. I benefited a lot from the help and the discussion with a post-doctoral fellow Dr. Francesco Macchioni and my colleagues Ms. Louise Longridge, Mr. Nate Petersen in the Paleontology and Jurassic Stratigraphy Laboratory.

Again, my sincerest thanks go to Paul L. Smith and Kate for their hospitality. Their enthusiasm made me feel at home as I adapted to a new environment.

Finally, I wish to express my thanks to my wife Nina, son Minqi, my parents and sisters, your love, encouragement, and dedicated support mean a great deal to me in my endeavors.

Chapter 1 Introduction

1.1 Introductory Statement

Based on the compilation of data for fossil invertebrate and vertebrate families, Raup and Sepkosk (1982) recognized five mass extinctions occurring in the Late Ordovician (end-Ashgillian), Late Devonian (Givetian-Frasnian), Late Permian (Guadalupian-Dzhulfian), Late Triassic (end-Norian), and Late Cretaceous (end-Maestrichtian) (Figure 1-1). The extinction at the end of the Triassic has long been recognized as significant, approximately equivalent in magnitude to the famous event at the end of Cretaceous when the dinosaurs and ammonites became extinct (Benton 1986).

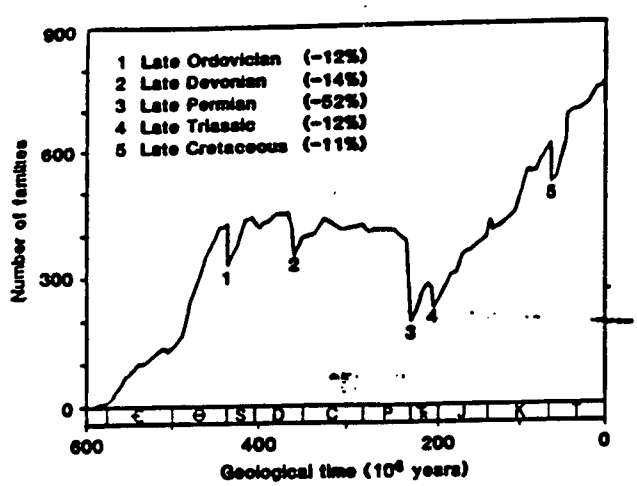

Figure 1-1 Five mass extinctions occurring in the Phanerozoic (Raup and Sepkosk, 1982)

The late Triassic mass extinction involved an overall reduction in the diversity of marine families by about 23% with a similar reduction in diversity of terrestrial families.

The effect on the ceratitid cephalopods was dramatic (all 46 late Triassic families died out) and the ammonoids barely survived into the Jurassic. When genera are considered, the Ceratitida reached a peak of about 150 genera in the Carnian, falling to about 100 genera in the Norian, and to single figures in the latest Norian (Benton 1986).

In this thesis, I examine the extinction and subsequent radiation of ammonoids during the Late Triassic and Early-Middle Jurassic, using univariate, bivariate, and simple multivariate techniques. The aims are to compare and contrast the evolution of Upper Triassic and Lower-Middle Jurassic ammonoid morphology and to explore the relationships among ammonoid morphospace, ornamentation, and suture types.

1.2 Purpose and Scope

This thesis focuses on morphological analysis of Upper Triassic and Lower-Middle Jurassic ammonoids in an attempt to establish the scope and rates of morphological change across the T/J boundary. The major goals of the thesis can be summarized as follows:

1. To assemble quantitative and qualitative morphology data for Upper Triassic - Middle Jurassic ammonoids.

2. To map the distribution of Upper Triassic and Lower-Middle Jurassic ammonites in terms of basic shell geometry so that relative densities of occurrence in different geometric regions can be evaluated and functional factors governing the distribution can be explored.

3. To detect possible covariations between whorl shape and basic morphological features.

4. To plot the low drag coefficient (C_D) values on the density contour maps of equidimensionally whorled ammonoids (WWWH = 0.9-1.1) so that the hydrodynamic efficiency of ammonoids from the Carnian Stage through Middle Jurassic can be evaluated.

5. To use the accumulated morphological range diversity index for basic ammonoid shell geometry and other ornamentation characters to document the style and rate of recovery in morphological diversity following the T-J extinction.

6. To chart the number of Late Triassic through Middle Jurassic heteromorph ammonoid species in order to document the duration between the extinction of heteromorph ammonoids in the Late Triassic and restoration of this aspect of morphological diversity in the Jurassic.

7. To map the distribution of different septal suture types on Carnian and Norian ammonite W-U plots in order to explore the relationships between the septal suture types and ammonoid geometry because there was a dramatic change in septal suture types across the Triassic-Jurassic boundary.

1.3 Introduction to Some Concepts

For the purpose of this thesis, there are three areas of research that are of some significance: 1) the evolution of ammonoid morphology; 2) the interrelations between morphology and hydrodynamics, which have potential evolutionary implications; 3) the contribution of computer databases to our understanding of morphology and morphologic change.

1.3.1 Modelling Ammonoid Shell Morphology

Raup (1966, 1967) in his two important papers established a numerical model to reflect the basic shell geometry of planispiral ammonites. He presented three fundamental parameters to describe the basic geometry of coiled shells: whorl expansion (W: which is the square of the ratio of radii), distance from the coiling axis (D in Raup's terminology, U used herein as umbilical ratio), and whorl shape (S in Raup's terminology, WWWH herein) (Figure 1-2).

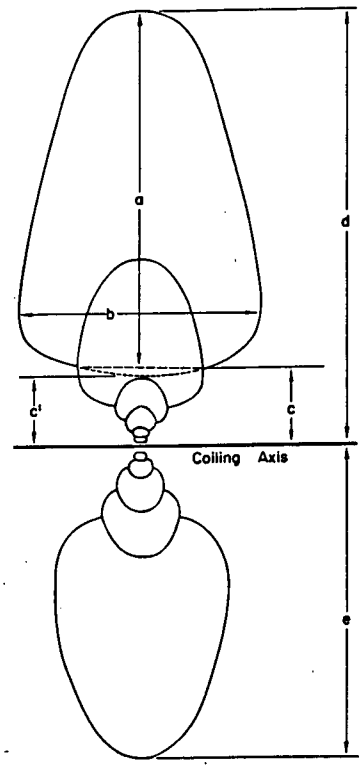

Figure 1-2 Linear dimensions measured for the calculation of the whorl expansion (W), umbilical ratio (U), and whorl shape in terms of compression and depression (WWWH). $W=(d/e)^2$; $U=c/d$; $WWWH=b/a$ (Raup, 1967)

Raup (1967) set up a spectrum of possible geometries, the W-U morphospace in which W and U are used to generate a W-U coordinate system (Figure 1-3). The distribution of hypothetical shell forms (computer produced) in W-U coordinate system

reflects the shell's coiling type and extent of overlap. The curved line of equation W = 1/U separates coiled forms with whorl overlap from those where whorls are separate.

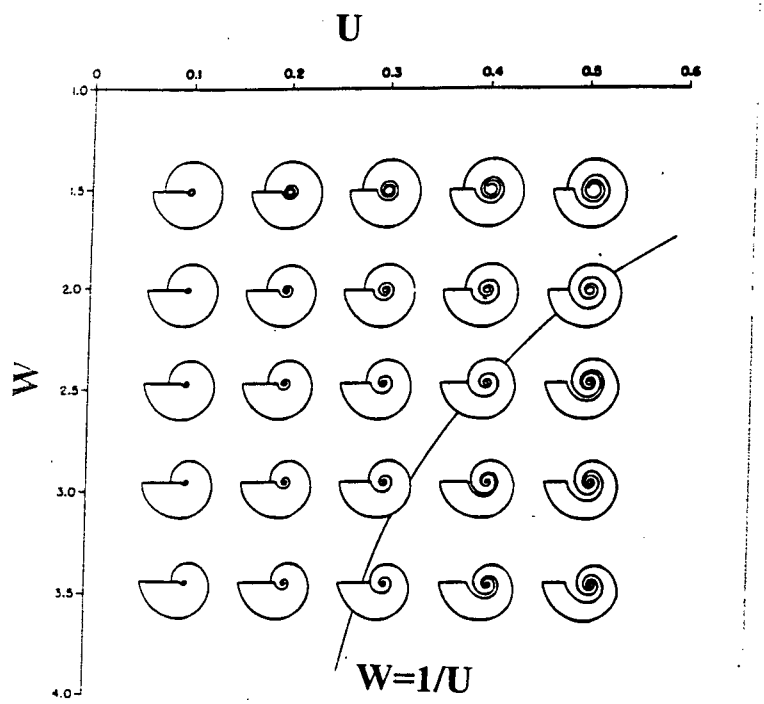

Figure 1-3 Hypothetical shell forms from the low W-low U corner of the planispiral ammonoid morphospace (Raup, 1967)

The W and U data for a set of ammonite samples can be plotted on the W-U coordinate system as a scatter diagram where one point represents one sample. The density of points in the scatter can be contoured and the result for the 405 genera of Paleozoic and Mesozoic planispiral ammonoids is shown in figure 1-4 (Raup, 1967). On this density-contoured map, 90% of the samples fall within the outermost contour line. The successively higher contours represent increase in points per unit area on the original plot. In this way, the theoretical spectrum inherent in an accreting shell model can be

compared with the "real world" of the fossil record. Uneven distributions are thought to have functional or evolutionary meaning.

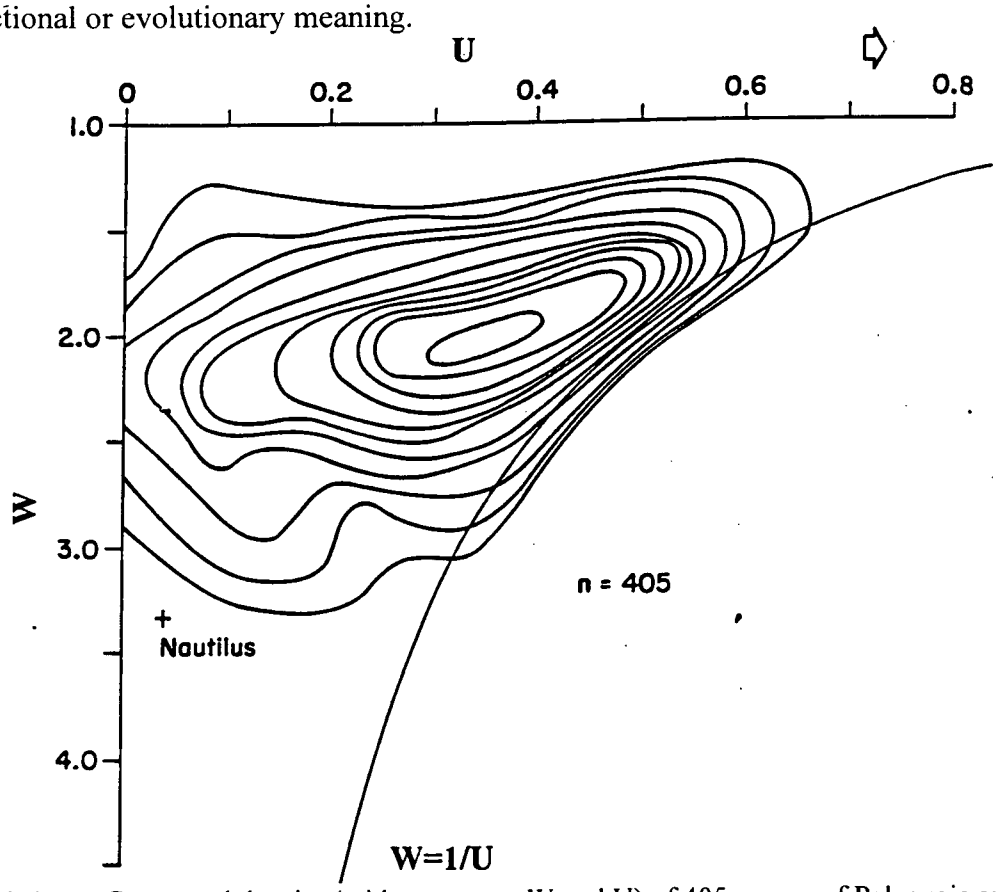

Figure. 1-4 Contoured density (with respect to W and U) of 405 genera of Paleozoic and Mesozoic planispiral ammonoids. 90% of samples lay within the outmost contour (Raup, 1967)

1.3.2 Interrelations between Morphology and Hydrodynamics

The hydrodynamic effect of ectocochliate cephalopod shell morphology has attracted the interest of ammonoid workers because the analysis of hydrodynamic efficiency provides the information for evaluating the palaeobiology of this important group of animals. When an object moves through a fluid, drag will be generated to resist the object's motion. A dimensionless number, the drag coefficient (C_D) is used to describe the drag producing capacity of a particular shape. The drag coefficient can be thought of as representing the hydrodynamic efficiency of an object. Chamberlain (1976) tested a

shell model in a current and visually analyzed the fluid flow. He suggested that most of the drag caused by a cephalopod derives from a few morphologic features of the shells. They are (1) the size of the umbilicus; (2) the width of the shell relative to its diameter (fineness ratio); (3) the size of the aperture.

By contouring a C_D data derived from his models, Chamberlain (1976, 1980) created a map which shows the effect of W and U on shell drag coefficient for shells

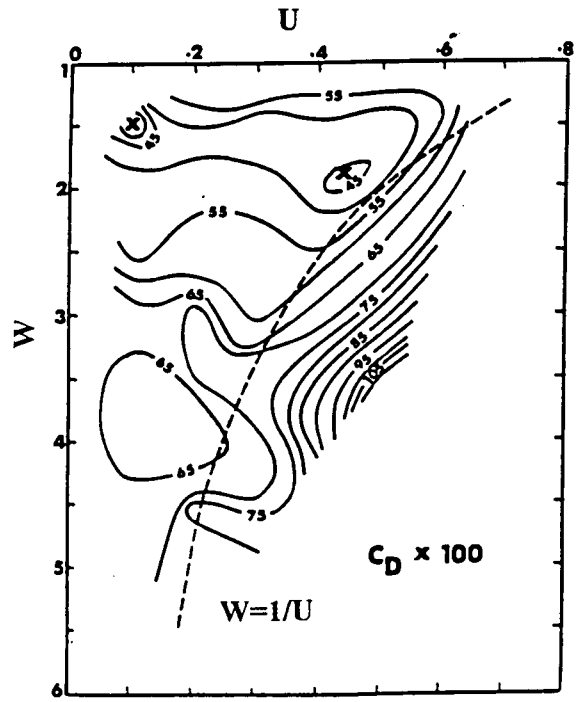

Figure. 1-5 Contour map of drag coefficient (x100), showing combined effect of W and U on C_D. C_D and geometrical data from Chamberlain (1976). Dashed line – offlap line (W=1/U). Xs mark geometries with lowest C_Ds and highest hydrodynamic efficiencies (Chamberlain, 1980)

having circular whorl cross section (WWWH=1). The result shows that there are two points of low C_D within the region (Figure 1-4). One is at W=1.5, U=0.1 and the other at W=2, U=0.43. These two points mark geometries with lowest C_Ds and highest hydrodynamic efficiency. I select a set of specimens with equidimensional whorl cross

sections (WWWH=0.9~1.1) and, for each stage of the Late Triassic through Middle Jurassic Bajocian, create W-U density contour maps. With the comparison of the highest contour peak positions of these maps and Chamberlain's C_Ds' position, a general impression of the interrelations between morphology and hydrodynamics through these stages can be approached.

1.3.3 Ammonoid Computer Databases

The application of computer databases to paleontology has made tremendous progress in recent years. The computer can be used in fossil identification by matching specimen figures or comparing morphological measurements or descriptions with those already stored in the database or it can be used to assemble a profile of the ontogenetic development of any species. Kullmann et al. (1991) developed a computer database "GONIAT" for storing Paleozoic ammonoid research information. Smith (1986) created a database management system called AMMON to systematically handle data accruing from stratigraphic studies of Jurassic sedimentary basins in North America. AMMON was expanded later to contain 7790 Jurassic ammonoid specimens representing 15 families, 179 genera and 1319 species (Liang and Smith, 1997). In AMMON, each specimen has 120 descriptors covering taxonomy, quantitative morphology, qualitative morphology, stratigraphy, locality information, and general comments. AMMON is essential to this study and its content was expanded to include the Upper Triassic, in addition to Lower and Middle Jurassic ammonoids.

1.4 Stage Divisions of Upper Triassic and Lower-Middle Jurassic

The stage divisions of the Upper Triassic series are summarized by Tozer (1994) who divides the Upper Triassic into Carnian and Norian stages, the latter including the Rhaetian Stage which is recognized as a separate stage by some workers (Haq et al., 1988; Harland et al., 1989; Odin, 1994; Gradstein et al., 1994). The Lower Jurassic and Middle Jurassic series are both divided into four stages (Table1-1).

Series	Stage	Age at base (m.y.)	Duration (m.y.)
Middle Jurassic	Callovian	Top: 156.5 (+3.1/-5.1) Base: 160.4 (+1.1/-0.5)	3.9
	Bathonian	166.0 (+3.8/-5.6)	5.6
	Bajocian	174.0 (+1.2/-7.9)	8.0
	Aalenian	178.0 (+1.0/-1.5)	4.0
Lower Jurassic	Toarcian	183.6 (+1.7 /-1.1)	5.6
	Pliensbachian	191.5 (+1.9/-4.7)	7.7
	Sinemurian	196.5 (+1.7/-5.7)	5.0
	Hettangian	199.6 (±0.4)	3.1
Upper Triassic	Norian	223.4	23.8
	Carnian	235.0	11.6

Table 1-1 Stage divisions for Upper Triassic through Middle Jurassic (base ages of Upper Triassic stages are from Harland et al., 1989; base ages of Lower and Middle Jurassic stages are from Pálfy et al., 2000)

Chapter 2 Shell Geometry through Time

2.1 Introduction

Through their long geological history, ammonoids evolved a diverse suite of shell morphologies in response to biological and environmental evolutionary pressures. Nearly all of these morphologies are represented within the time interval under discussion but they are far from evenly distributed. In this chapter, changes in basic shell morphology from the Late Triassic to the Middle Jurassic are explored using a simple multivariate model developed by Raup (1966). This model describes a continuous spectrum of potential shell geometry producing a "morphospace" whose stage-by-stage occupation can then be explored using the data from the database AMMON and published literature.

As mentioned in the previous chapter, Raup (1966) established a numerical model to reflect the basic shell geometry of planispiral ammonites. Three parameters are used in this model (Figure 1-2). They are whorl expansion rate (W), umbilical ratio (U), and shape of whorl (WWWH). W and U can be used to generate a W-U coordinate system. The distribution of hypothetical shell forms (computer produced) in W-U coordinate system reflects the shell's coiling type and extent of overlap. A curved line of equation W=1/D separates coiled forms with whorl overlap from those where whorls are separate.

The W and U data for a set of ammonoid samples can be plotted on the W-U coordinate system as a scatter diagram where one point represents one sample. The

density of points in the scatter can be contoured to create a density-contoured map. On this density-contoured map, most of the data falls within the outermost contour line. The successively higher contours represent increasing points per unit area on the original plot. The purpose of this chapter is to explore the distribution of the Upper Triassic Carnian Stage through Middle Jurassic Bajocian Stage ammonoids in terms of basic shell geometry (W and U) so that the relative densities of occurrence in different geometric regions can be evaluated through time and functional factors governing the distribution can be explored.

2.2 Data Sources and Sampling

The Late Triassic Carnian and Norian stage ammonite measurements used in this study are taken from the plaster specimens and figures in the work of Tozer (1994), Wiedmann (1973), Rakús (1993). The data of Lower and Middle Jurassic ammonites are taken from the AMMON database, Guex (1995), Smith and Tipper (1996, 2000), Bloos (1999), Bloos et al. (2000), Schlegelmilch (1985), Stuttgart (1978). The type species for each genus was based on information in Arkell et al. (1957) and Donovan et al (1981, 1998).

A few factors affect the results of statistics-related research in paleontology. First, acceptable illustrations, real fossils, or plaster-cast specimens must be available so that the measurements can be made. Second, ontogenetic variations in geometry should be considered. Third, taxonomical bias should be minimized. Despite the rapidly improving database, it is still not possible to undertake a complete study at the species level because

some species are poorly defined and many are synonyms. To overcome this problem, our study is made at the genus level where completeness is possible. In order to reduce statistical bias and minimize other shortcomings, samples are chosen on the basis of the following criteria: 1) For each genus, at most only eleven species are selected, including the type species. This limits the statistical bias of those genera with high number of species, many of which may not be valid. Species other than types are selected randomly (by randomly selecting numbers which represent different species); 2) Only one sample is selected for each species. If the species has more than two samples, the following priorities are followed: (i) holotype specimen; (ii) the best preserved specimen; (iii) the sample having the most complete measurements; (iv) the sample with the largest diameter, which reduces the impact of ontogenetic change on the data.

2.3 Occupation of Shell Geometry Morphospace

Using the sampling strategy described in 2.2, ammonoid species were selected from Upper Triassic Carnian through Middle Jurassic Bajocian stages. By using Raup's approach on ammonoid shell geometry (Raup, 1967) and with the application of SURFER program, contoured W-U density maps for each stage were constructed (Figure 2-1 to 2-8). In addition, three-dimensional W-U density surface plots were correspondingly established (Figure 2-9 to 2-16). SURFER is a grid-based contouring and three-dimensional surface plotting graphics program that runs under Microsoft Windows. SURFER interpolates irregularly spaced XYZ data onto a regularly spaced grid. In our research, XYZ data refers to the geometric parameters W, U, and their

density number in a certain unit area. These interpolated data are placed in a grid [.GRD] file. The grid file is then used to produce contour map and three-dimensional surface plot. On our W-U density contour maps and three-dimensional surface plots, the curved line of W=1/U is overlaid so that the territories of overlap-whorl shells (W<1/U) and loose-coiled shells (W>1/U) can be clearly viewed.

2.4 Ammonoid Shell Geometry by Stage

Carnian Stage: 122 samples represent 122 species belonging to 63 genera. Figure 2-1 and Figure 2-9 are the results of W-U contoured density map and the three-dimensional density surface plot for the planispiral ammonoids from the Carnian Stage. The contour plot is characterized by multi-peaks. The two highest peaks occur at relatively low U values (around U=0.3 and 0.35) with W values of 1.87 and 2.30. Low U values indicate that the Carnian Stage ammonoids are generally involute forms.

Norian Stage: 184 samples represent 184 species of 82 genera. The W-U density contour map (Figure 2-2) and three-dimensional surface plot (Figure 2-10) for the Norian Stage ammonoids show a similar pattern compared with the Carnian Stage, but the contoured area distributes over two sides of the W=1/U curve because of the existence of a few heteromorph ammonoid genera in the Norian Stage, such as *Vandaites* and *Choristoceras.* These types of ammonoids are normally uncoiled. A few of the density peaks distribute along the W axis and their W range is between 1.6-2.7. Another high peak has a relatively high W value and its position is W=2.22 and U=0.38.

Hettangian Stage: 103 specimens representing 103 species and 33 genera were selected to produce their W-U density contour map (Figure 2-3) and three-dimensional surface plot (Figure 2-11). The diagram shows an oval pattern along the W=1/D curve. The highest peak is located at W=1.85 and U=0.40.

Sinemurian Stage: A W-U density contour map (Figure 2-4) and a three-dimensional surface plot (Figure 2-12) were made based on 166 specimens that represent 166 species of 49 genera. The highest peak has a smaller W value (about 1.65) and a larger U value (0.57). This indicates that the majority of the Sinemurian ammonites were more evolute and their whorls more slowly expanding than those in the Hettangian Stage.

Pliensbachian Stage: 323 specimens representing 323 species of 65 genera in the Pliensbachian Stage were used to produce a W-U contour density map (Figure 2-5) and a three-dimensional surface plot (Figure 2-13). The position of the peak is at W=1.80 and U=0.55.

Toarcian Stage: In this stage, there are 294 W-U points (representing 294 species of 58 genera) having been selected to create a density contour map (Figure 2-6) and a three-dimensional surface plot (Figure 2-14). The peak is at W=1.95 and U=0.45.

Aalenian Stage: 62 samples representing 62 species of 24 genera are selected to create a W-U contoured density map (Figure 2-7) and a three-dimensional surface plot for this stage (Figure 2-15). The diagrams still show an oval shape but the position of peak has a relatively high W value (2.20) and low U (0.35).

Bajocian Stage: A W-U contoured density map (Figure 2-8) and a three-dimensional surface plot (Figure 2-16) were constructed based on 68 specimens that

represent 68 species of 61 genera in the Bajocian stage. The heteromorph ammonoids appeared again in this stage (e.g. *Spiroceras*) so that the contoured area extends to the other side of the W=1/U curve (distributes at the region of W>1/U). This is the earliest stage that heteromorphic ammonoids can be found again since the end-Triassic mass extinction. The peak of the W-U density diagrams is W=2.20 and U=0.25.

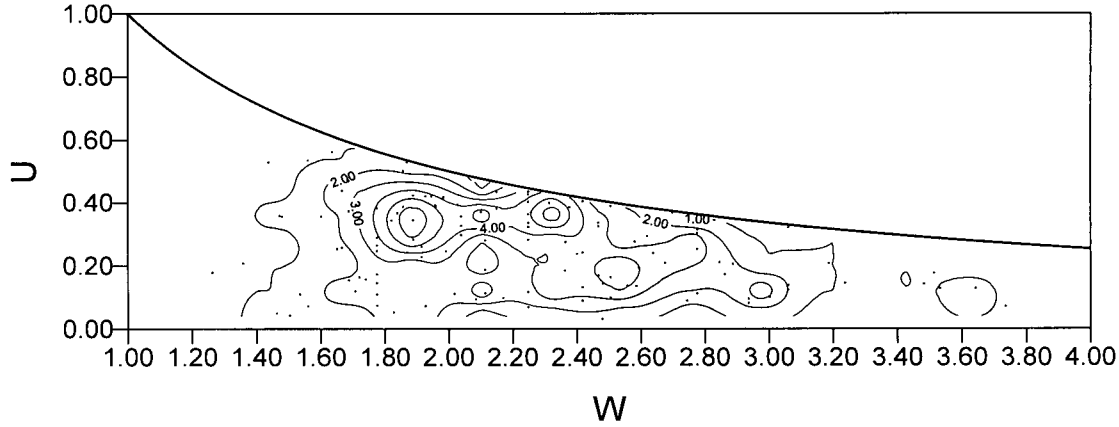

Figure 2-1 Contoured density diagram for Carnian ammonoids (N=122)

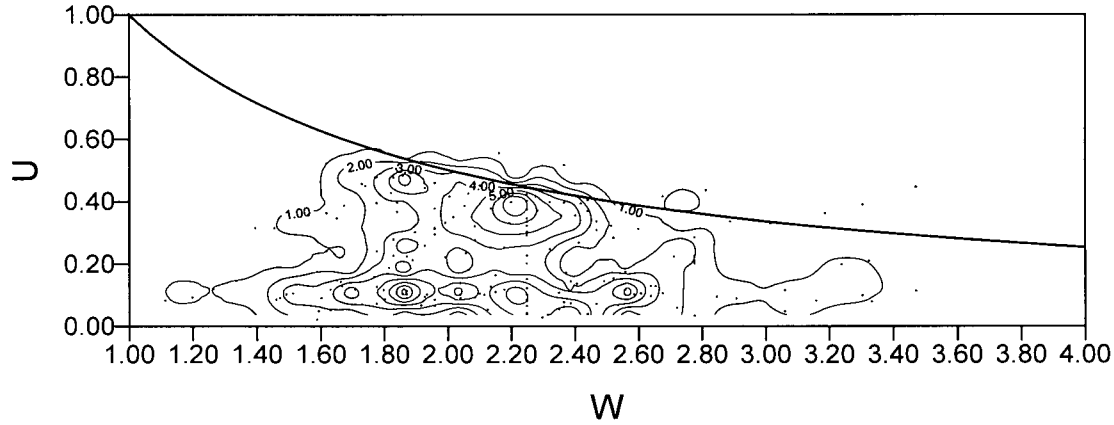

Figure 2-2 Contoured density diagram for Norian ammonoids (N=184)

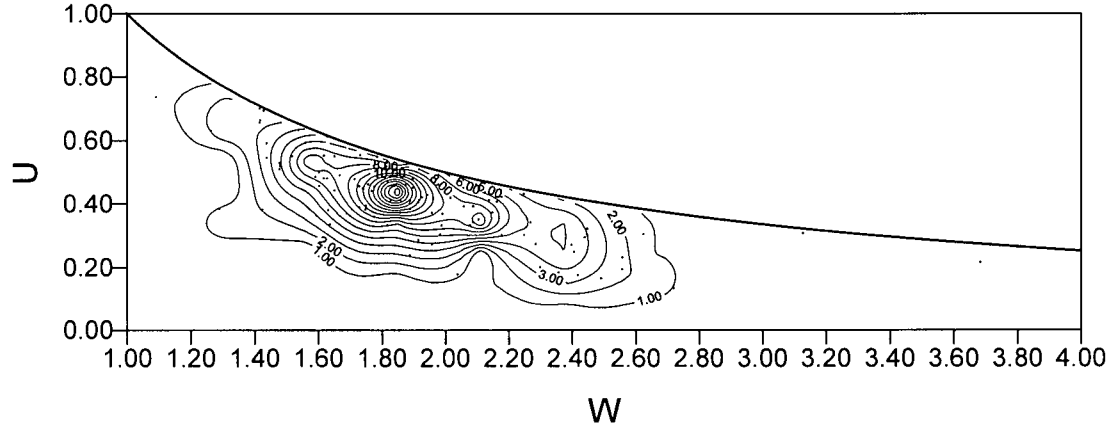

Figure 2-3 Contoured density diagram for Hettangian ammonoids (N=103)

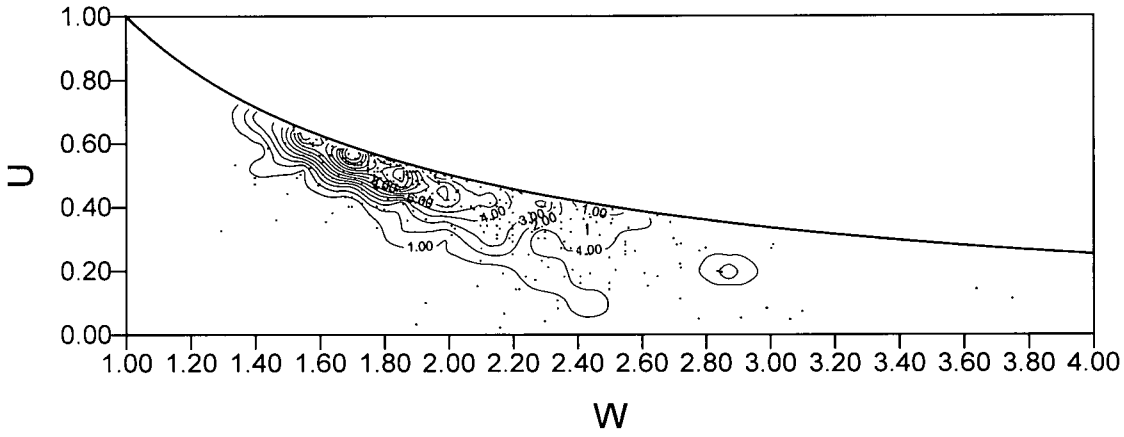

Figure 2-4 Contoured density diagram for Sinemurian ammonoids (N=166)

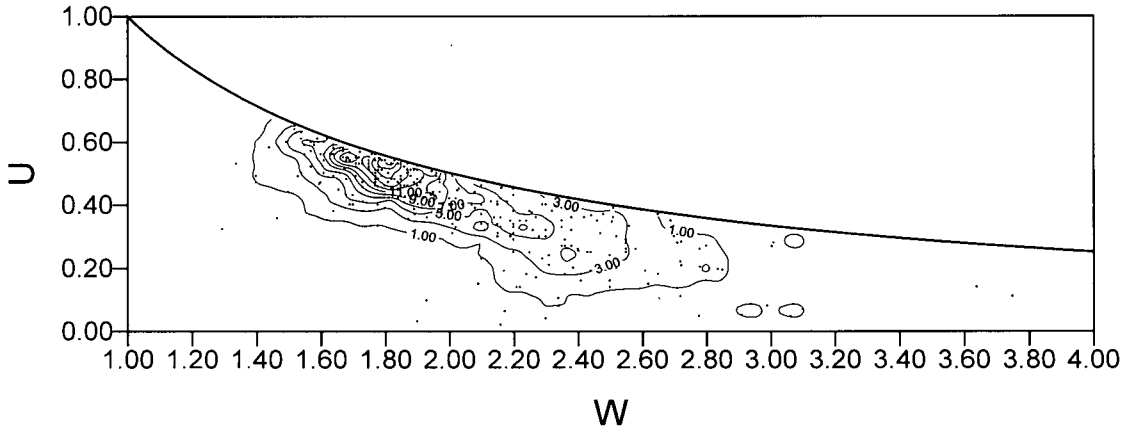

Figure 2-5 Contoured density diagram for Pliensbachian ammonoids (N=323)

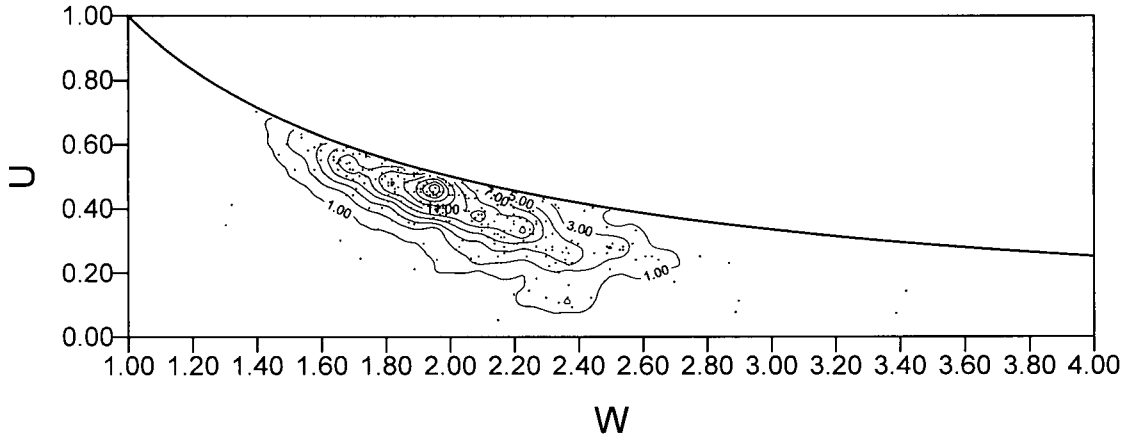

Figure 2-6 Contoured density diagram for Toarcian ammonoids (N=294)

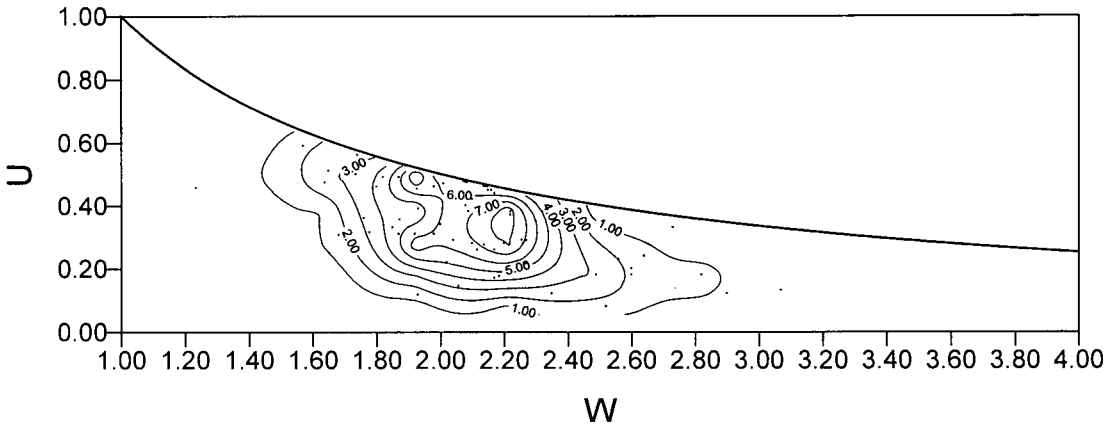

Figure 2-7 Contoured density diagram for Aalenian ammonoids (N=62)

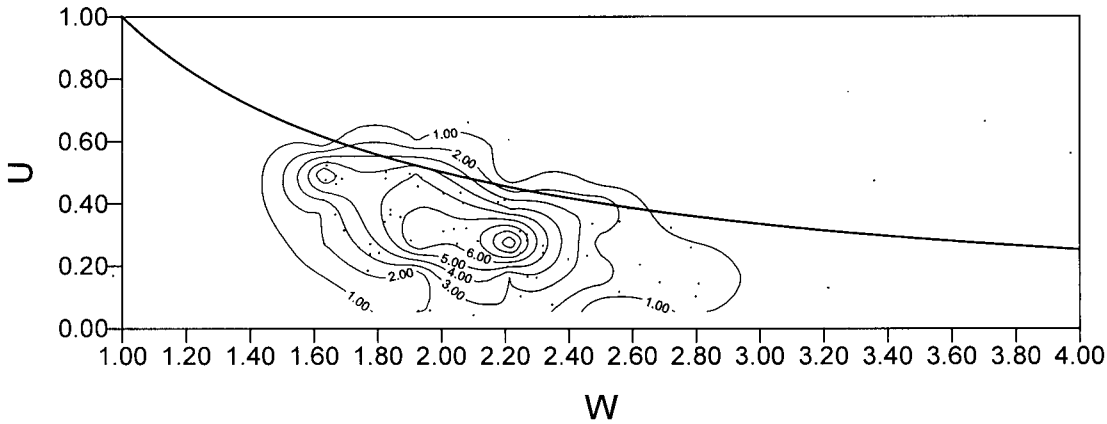

Figure 2-8 Contoured density diagram for Bajocian ammonoids (N=68)

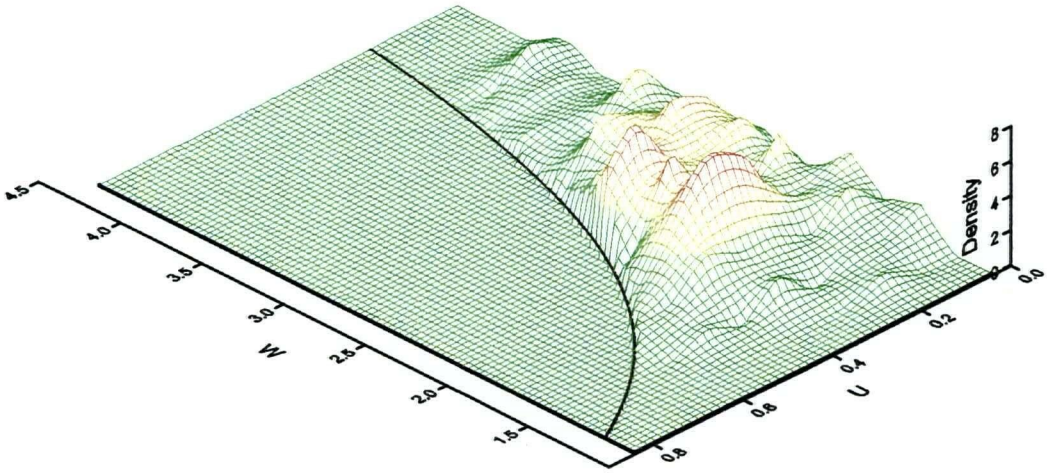

Figure 2-9 3-D density diagram for Carnian ammonoids (N=122)

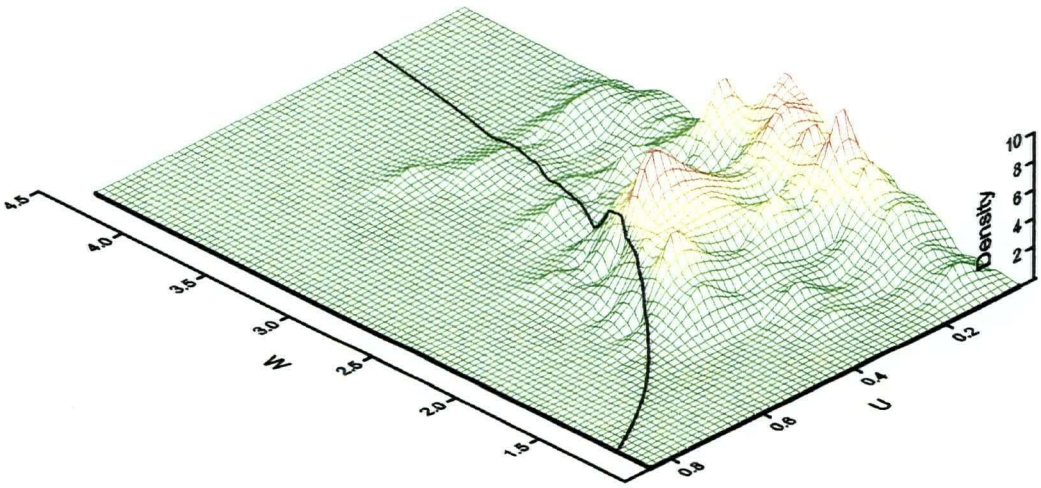

Figure 2-10 3-D density diagram for Norian ammonoids (N=184)

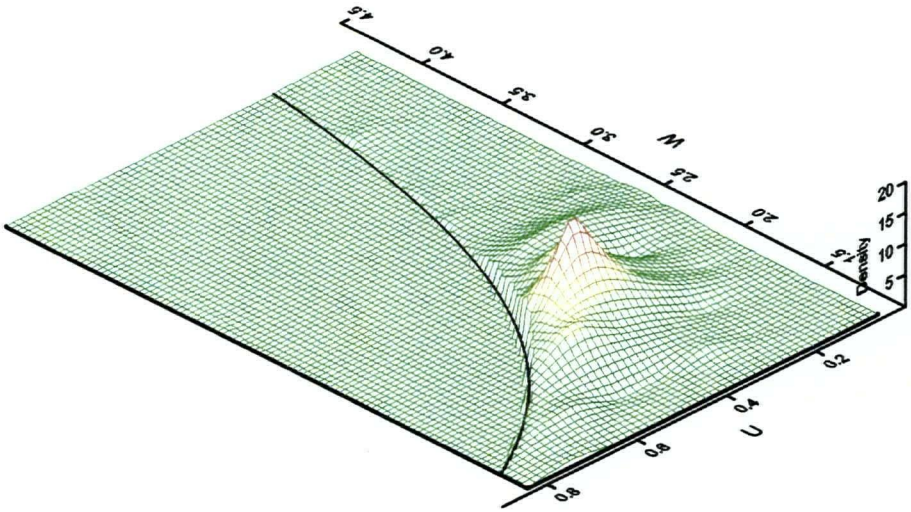

Figure 2-11 3-D density diagram for Hettangian ammonoids (N=103)

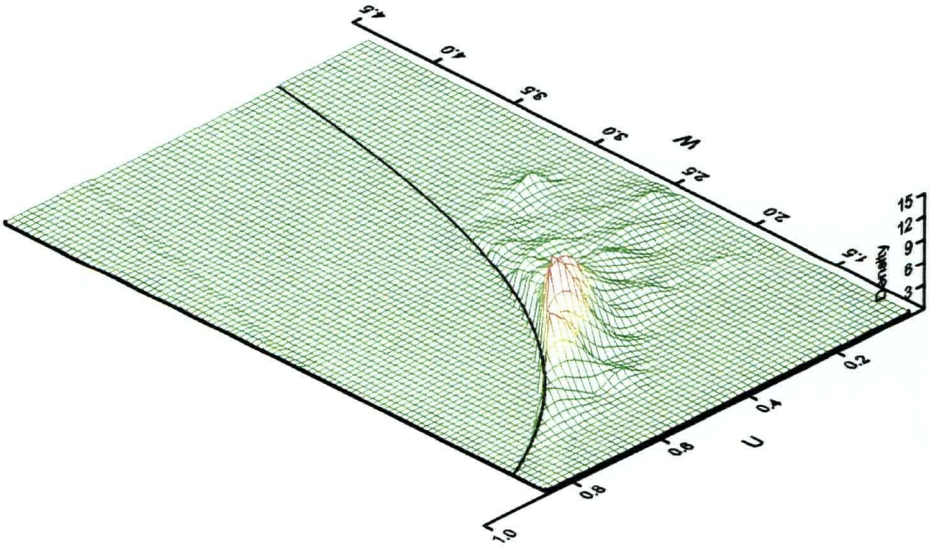

Figure 2-12 3-D density diagram for Sinemurian ammonoids (N=166)

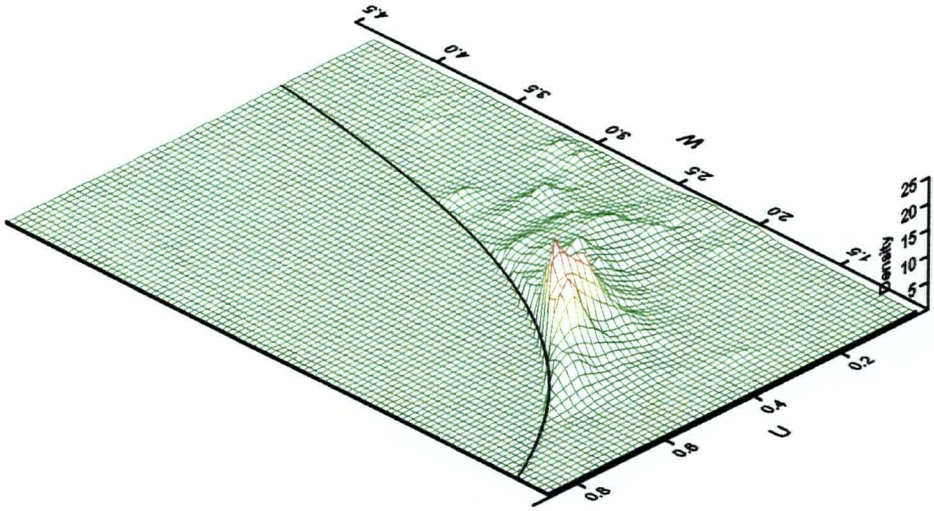

Figure 2-13 3-D density diagram for Pliensbachian ammonoids (N=323)

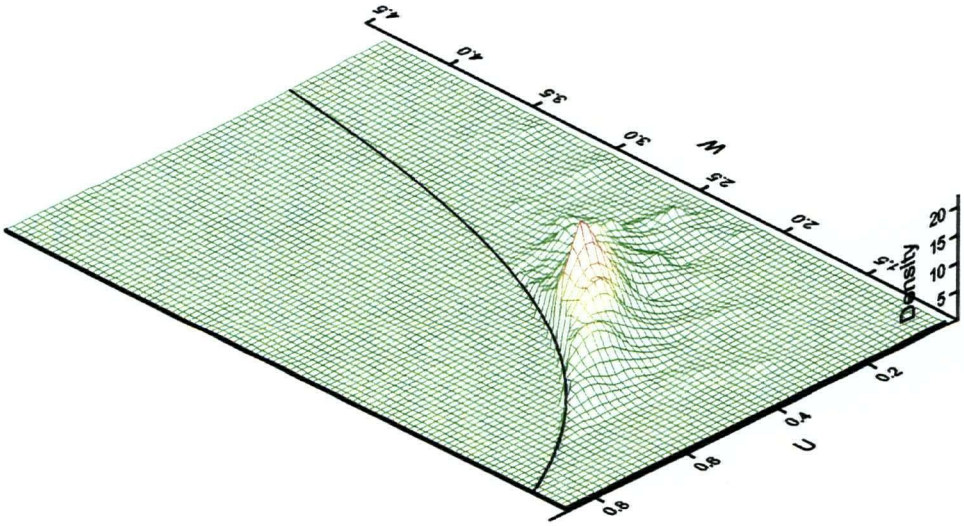

Figure 2-14 3-D density diagram for Toarcian ammonoids (N=294)

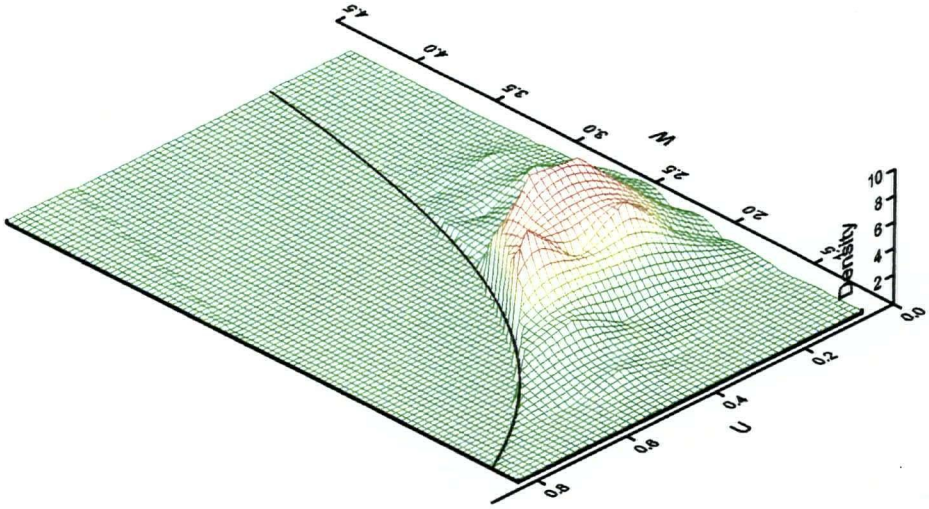

Figure 2-15 3-D density diagram for Aalenian ammonoids (N=62)

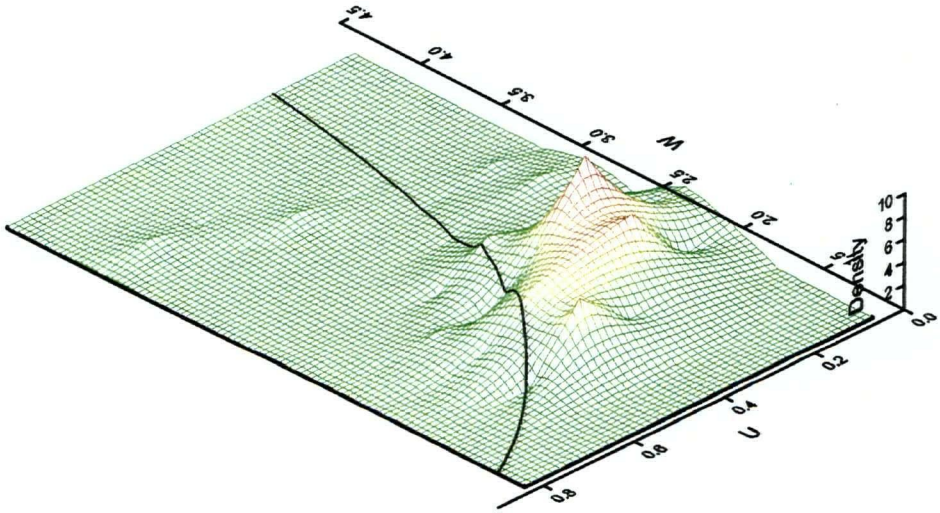

Figure 2-16 3-D density diagram for Bajocian ammonoids (N=68)

2.5 Buckman's Law of Covariation

It is important to find out whether certain combinations of values of the several parameters confer an advantage and increase the frequency of that geometry in the fossil record. That is particularly important while considering the effect of a major extinction.

By studying the extraordinarily rich and morphologically varied *Sonninia* fauna from the Sowerbyi Zone of the Bajocian Stage of Dorset in England, Buckman (1892) observed covariation among shell coiling, whorl section, and shell ornament: "Roughly speaking, inclusion of the whorls correlate with the amount of ornament - the most ornate species being the most evolute, and having almost circular whorls". This observation was named as "Buckman's law of covariation" by Westermann (1966) who reassessed this *Sonninia* assemblage and concluded: 1) The correlation of whorl compression (WWWH) and relative umbilical width (U) is significantly positive; 2) Whorl width (WW) and relative umbilical width (U) are not clearly inter-correlated but show positive shift of maximum values. 3. The whorl section (WWWH) plotted against number of primaries (as PRHW in AMMON database, representing the number of primary ribs per half whorl) shows a weak positive correlation. Westermann's further observations can be considered an extension of "Buckman's law of covariation". However, since the "Buckman's law of covariation" was established for a group of Middle Jurassic Hildoceratids, the question arises: does this "law" apply to other ammonoid groups or the groups that existed before the end-Triassic extinction?

2.6 Discussion

W and U have been chosen as two geometric parameters to create the above contoured density diagrams from Late Triassic Carnian Stage through Middle Jurassic Bajocian Stage. A goal is to determine whether W and U are correlated with each other. Buckman's law describes the correlation among shell coiling, whorl section, and shell ornamentation. Raup's contoured density (with respect to W and U) of natural occurrences of Paleozoic and Mesozoic 405 planispiral ammonoid genera selected from *Treatise on Invertebrate Paleontology* (Arkell et al., 1957) shows that the correlation between W and U is negative (Raup, 1967). The contoured W-U diagrams from Hettangian through Bajocian stages in this thesis show similar patterns. They are unimodal and have only one major distinct peak on each diagram. A negative relationship exists in their W-U distributions, which agrees with the Buckman's law and the result of Raup (1967). However, the contoured W-U diagrams of Carnian stage and Norian stage are different from those of Early and Middle Jurassic stages. The distribution is broad, nonlinear and with multi-peaks on W-U density distribution. There is no apparent negative correlation between W and U with Carnian and Norian stages. Our research showes that Buckman's law is apparently applicable to Jurassic ammonoids, but weakly to Late Triassic ammonoids.

Heteromorph ammonoids are a type of ammonoid with shells that are uncoiled or deviate from a plane spiral. Raup (1966) created shell forms with the application of a computer to illustrate the spectrum of possible shell forms (Figure 2-17). A parameter "translation rate (T)" is introduced to describe the coiling of the tube down the spiral axis.

The translation rate is measured as the ratio of the vertical movement to the lateral movement during rotation about the coiling axis (Figure 2-18). I counted the number of heteromorph ammonoid species from Upper Triassic through Middle Jurassic (Figure 2-19). Among these heteromorph ammonoids, four types of geometry can be seen: straight,

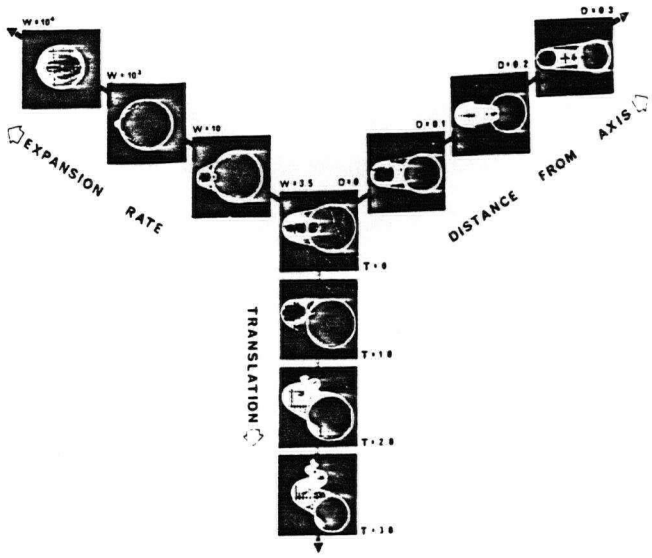

Figure 2-17 The morphological effects of change in whorl expansion rate (W), translation rate (T), and the distance from the generating curve to the axis (D in Raup's terminology, U used herein as umbilical ratio) (Raup, 1966)

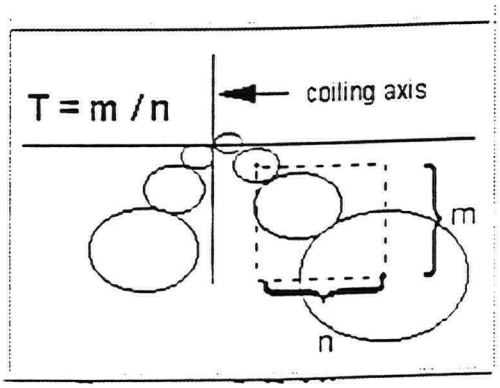

Figure 2-18 Measurement of the translation rate (T)

curved, loose-sprial, and helicospiral. Fourteen heteromorph species belonging to six genera *Vandaites, Choristoceras, Peripleurites, Rhabdoceras, Paracochloceras* and *Cochloceras* are found in the Norian Stage. Eight species, all belonging to the genus *Spiroceras* (which includes *Apsorroceras*, Schlegelmich, 1985), occur in the Bajocian Stage. Two species belonging to *Parapatoceras* occur in the Bathonian stage. Seven species belonging to the genera *Parapatoceras* and *Acuariceras* occur in the Callovian Stage. The Norian Stage not only has the most heteromorph ammonoid species and genera, but also has all the four types of spiral patterns. In Middle Jurassic stages, the number of heteromoph ammonoid species and genera is relatively small, and there are no helicospiral ammonoids.

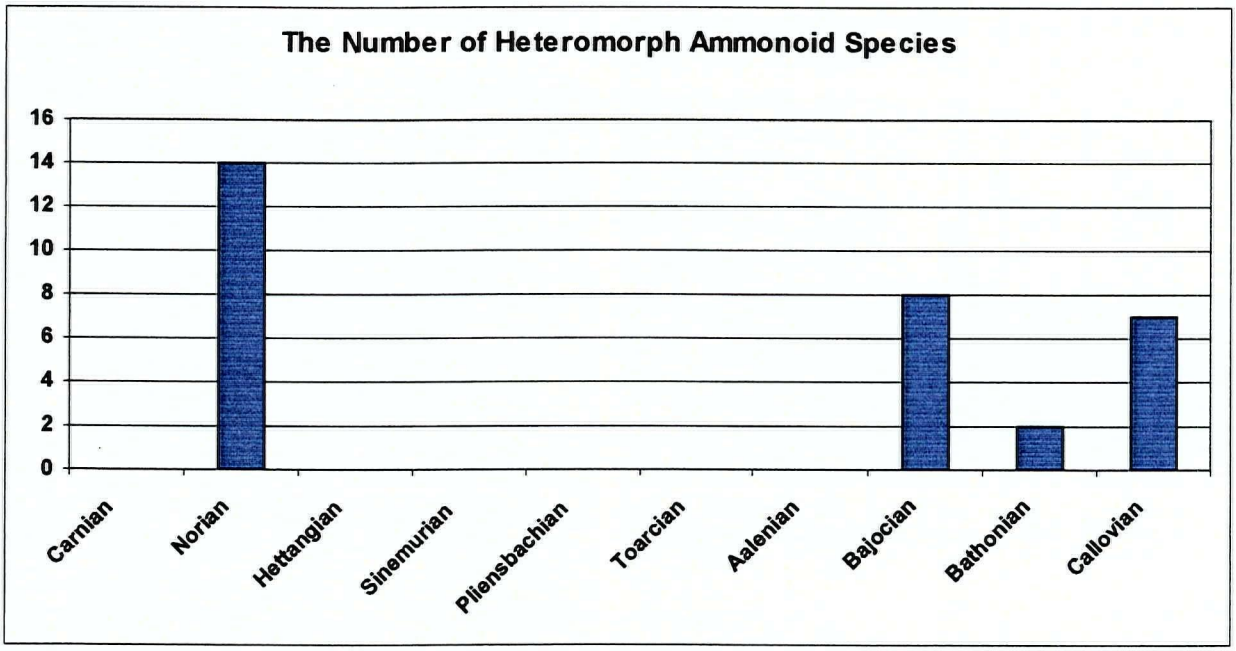

Figure 2-19 The number of heteromorph ammonoid species from Carnian Stage through Callovian Stage

In summary, the evolution of ammonoid shell geometry through the end-Triassic extinction is a thorough remoulding process. This is evident in two ways:

1. The geometry of ammonoid shells is different at pre-extinction and post-extinction. Before the extinction, in the Upper Triassic Carnian and Norian stages, the W-U density diagrams show a broad, nonlinear, and multi-peaked pattern. The peaks are distributed in relatively low U regions. The negative correlations between W and U are not apparent. In contrast, in the Early Jurassic post-extinction period, the W-U density diagrams show a narrow, linear plot with only one obvious peak. The correlation of W and U is obviously negative. The densities concentrate in areas of high U values. In the Middle Jurassic Aalenian and Bajocian stages, the patterns of W-U density become broader. Although the negative correlation between W and U still exists, it is not so obvious as in Early Jurassic faunas. High W-U density locates in areas of relatively low U values. So the general pattern is close to that in the Upper Triassic.

2. Heteromorph ammonoids underwent a convincing evolution. In the Norian Stage of the Late Triassic, the diversity of heteromorph species and genera is high, with fourteen species belonging to six genera. The types of spiral patterns are varied: straight, curved, loose-sprial, and helicospiral. Heteromorph ammonoids do not occur in the Early Jurassic and it is not until the Bajocian Stage of the Middle Jurassic that heteromorph ammonoids appeared again and even then the diversity of species and genera is low. Only three heteromorph genera in total are found in the Middle Jurassic, and there was no helicospiral spiral form. Based on the above, three stages can be recognized with respect to shell geometry through time:

1. Late Triassic (pre-extinction interval, including Carnian and Norian stages): broad, nonlinear, and multi-peaked geometry pattern; low U W-U density regions; no obvious negative correlations between W and U; high diversity heteromorph ammonoid with four types of shell geometries.

2. Early Jurassic (post-extinction interval, including Hettangian, Sinemurian, Pliensbachian, and Toarcian stages): narrow, linear, and one obvious peak geometry pattern; high U W-U density regions; negative correlation between W and U; no heteromorph ammonoids.

3. Middle Jurassic (recovery interval, including Aalenian and Bajocian stages): broad, not obvious linear geometry pattern; low U W-U density; weak negative W-U correlation; low diversity heteromorph ammonoids and three spiral patterns (no helicospiral shells).

Chapter 3 Morphological Covariation between Whorl Shape and Shell Geometry

3.1 Introduction

As previously mentioned in Chapter 2, "Buckmann's law of covariation" describes the covariation relationship among shell coiling, whorl section, and shell ornamentation which in turn may have a bearing on shell function and evolutionary success. As described in Chapter 1, Raup (1966, 1967) presented three fundamental parameters by using a numerical model to describe the basic geometry of coiled shells: whorl expansion (W), distance from axis (U used herein as umbilical ratio), and whorl shape (WWWH). The purpose of this chapter is to explore possible covariations between whorl shape WWWH and the basic morphological features W and U because these covariations concern many speculations on relationships between shell shape and function.

3.2 Data and Sampling

The data sources used in this chapter are the same as those used in Chapter 2. However, since a few of samples do not have available WWWH data, other specimens are selected to replace them. If replacements are not available, these samples are removed.

3.3 Variations in Whorl Shape with Respect to W and U

By using Raup's approach (1967) on three fundamental parameters that describe the basic geometry of coiled shells, the contoured WWWH density maps with respect to W and U from the Carnian Stage of Upper Triassic through the Bajocian Stage of Middle Jurassic (Figure 3-1 to Figure 3-8) were created. On these maps, the darker areas indicate more compressed shells with lower WWWH values, whereas the lighter areas indicate higher WWWH value.

Carnian Stage: 113 specimens are selected to indicate 113 species of 63 genera. The general WWWH density pattern (Figure 3-1) shows that WWWH values increase in low-W and high-U regions, and decrease in high-W and low-U regions. Two high peaks are located at W=1.65 and U=0.25, and W=2.0 and U=0.41.

Norian Stage: 170 specimens indicating 170 species of 85 genera are selected. This stage has the similar WWWH density pattern as the Carnian Stage. The highest WWWH peak is at W=1.38 and U=0.33 (Figure 3-2).

Hettangian Stage: 69 specimens are sampled, which represent 69 species belonging to 27 genera. Multi-peaks display on the map. The highest two peaks are at W=1.82 and U=0.52, and W=2.45 and U=0.3 (Figure 3-3).

Sinemurian Stage: 119 samples represent 119 species of 41 genera, The peak is at W=2.15 and U=0.35 (Figure 3-4).

Pliensbachian Stage: 249 samples are selected to be representatives of 249 species of 55 genera. There are several peaks, but the highest peaks distribute on the area of W=1.5-2.0, U=0.4-0.5 (Figure 3-5).

Toarcian Stage: 251 specimens are used in this part. They represent 251 species belonging to 55 genera. The highest peak is at W=1.6, U=0.43 (Figure 3-6).

Aalenian Stage: 35 samples represent 35 species of 18 genera. High density distributes at the area of W=1.7-1.8 and U=1.5 (Figure 3-7).

Bajocian Stage: 56 samples indicate 56 species belonging to 51 genera. There are two distinguish peaks. One is at W=1.7 and U=0.48, and the other one is at W=2.68 and U=0.15 (Figure 3-8).

3.4 U-WWWH Contoured Density Diagrams

By using the same samples as above, the U-WWWH contoured density maps for the Carnian Stage through to the Bajocian Stage (Figure 3-9 to Figure 3-16) were created to discover if there are any correlations with the combinations of U and WWWH values.

3.5 W-WWWH Contoured Density Diagrams

The W-WWWH contoured density maps are constructed (Figure 3-17 to Figure 3-24) based on above samples. The correlations between W and WWWH can now be observed.

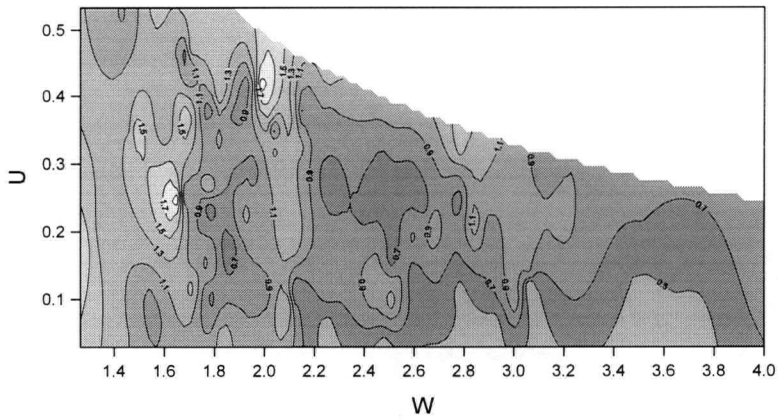

Figure 3-1 Contoured WWWH density with respect to W and U for Carnian ammonoids (N=113)

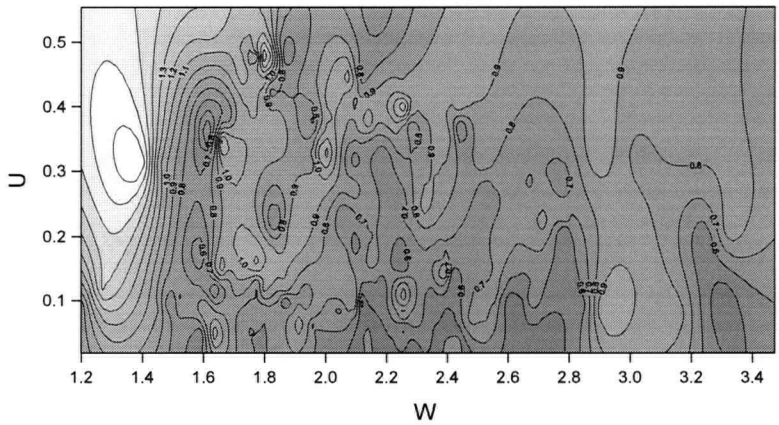

Figure 3-2 Contoured WWWH density with respect to W and U for Norian ammonoids (N=170)

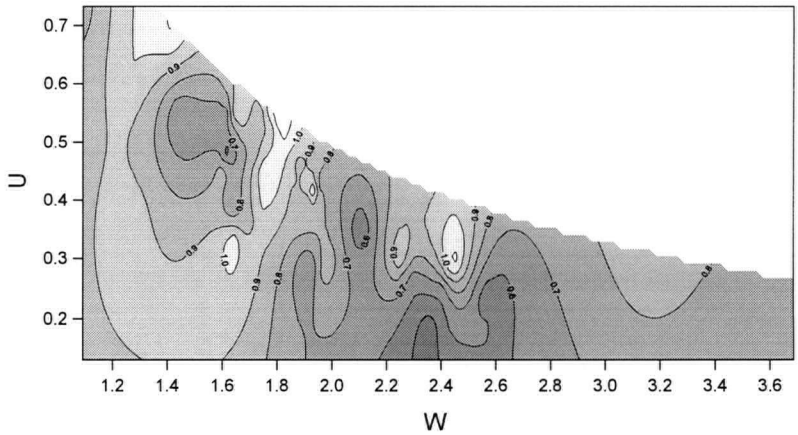

Figure 3-3 Contoured WWWH density with respect to W and U for Hettangian ammonoids (N=69)

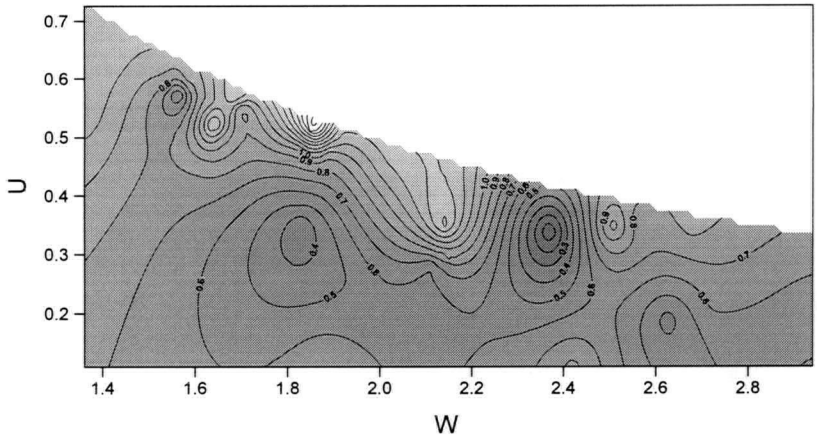

Figure 3-4 Contoured WWWH density with respect to W and U for Sinemurian ammonoids (N=116)

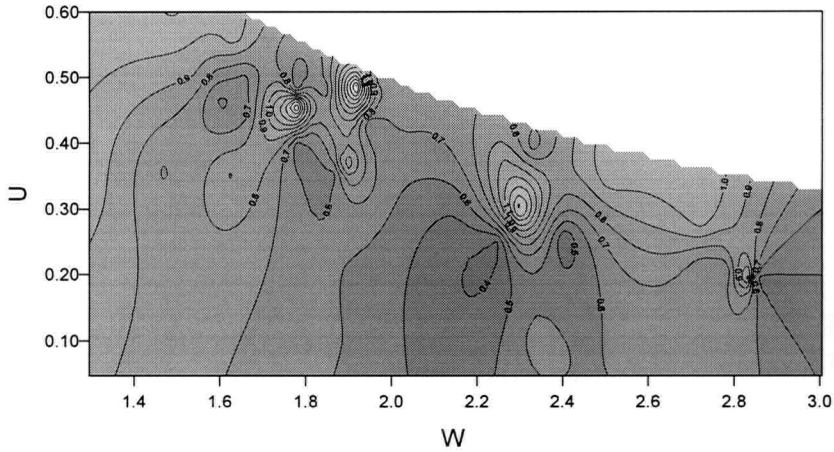

Figure 3-5 Contoured WWWH density with respect to W and U for Pliensbachian ammonoids (N=249)

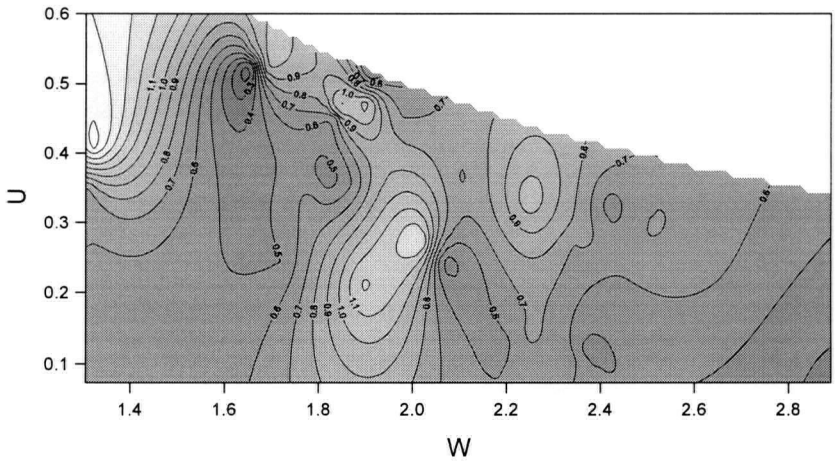

Figure 3-6 Contoured WWWH density with respect to W and U for Toarcian ammonoids (N=250)

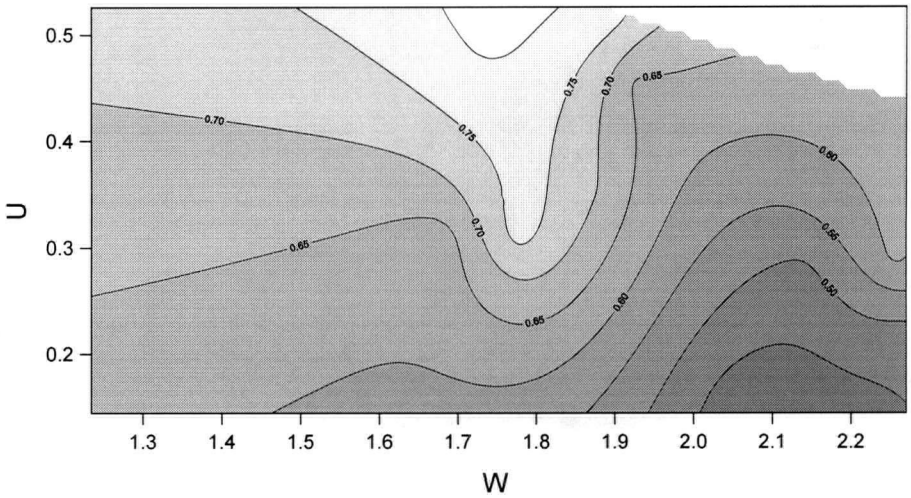

Figure 3-7 Contoured WWWH density with respect to W and U for Aalenian ammonoids (N=35)

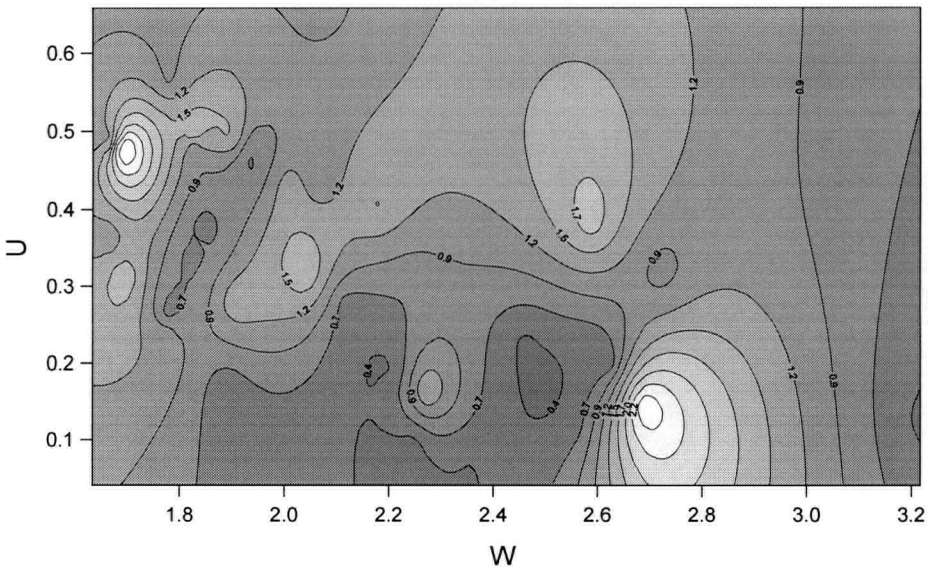

Figure 3-8 Contoured WWWH density with respect to W and U for Bajocian ammonoids (N=56)

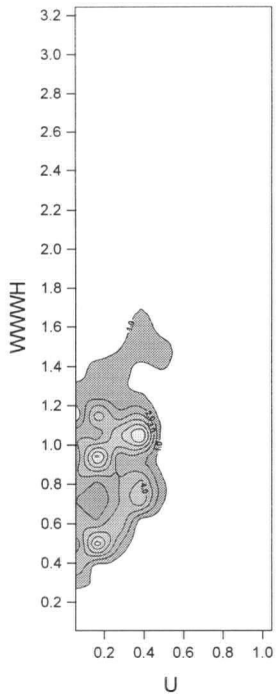

Figure 3-9 U-WWWH contoured density for Carnian ammonoids (N=113)

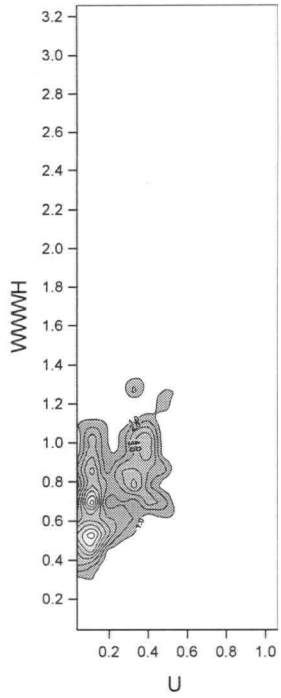

Figure 3-10 U-WWWH contoured density for Norian ammonoids (N=170)

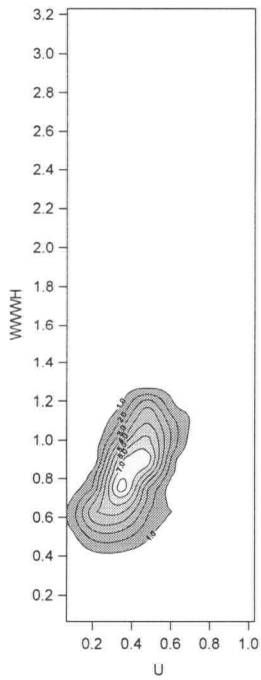

Figure 3-11 U-WWWH contoured density for Hettangian ammonoids (N=69)

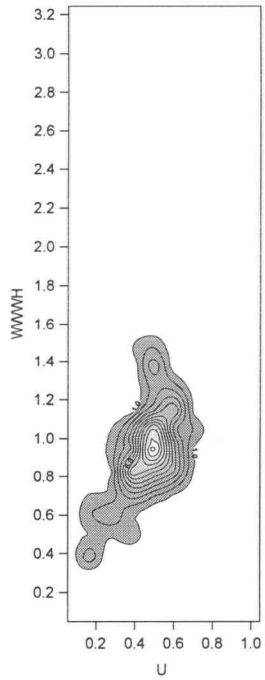

Figure 3-12 U-WWWH contoured density for Sinemurian ammonoids (N=116)

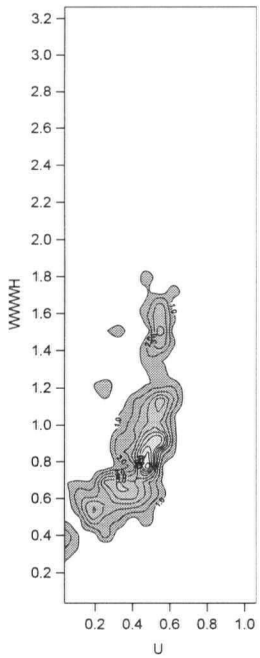

Figure 3-13 U-WWWH contoured density for Pliensbachian ammonoids (N=249)

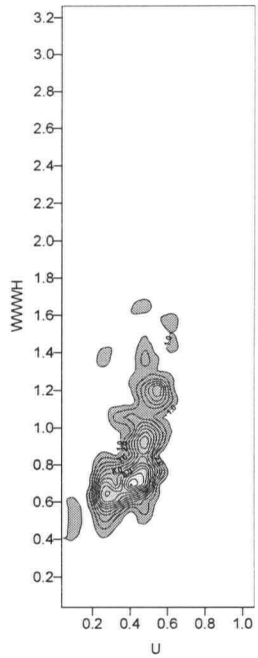

Figure 3-14 U-WWWH contoured density for Toarcian ammonoids (N=250)

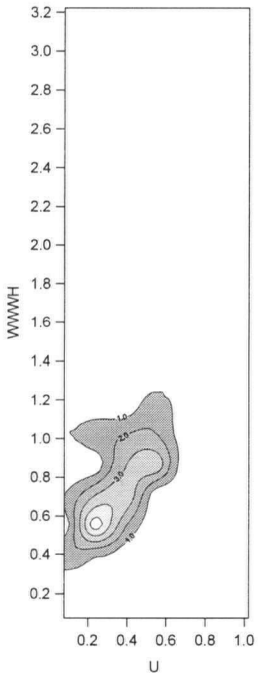

Figure 3-15 U-WWWH contoured density for Aalenian ammonoids (N=35)

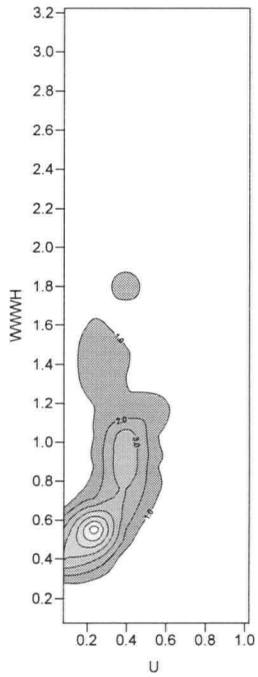

Figure 3-16 U-WWWH contoured density for Bajocian ammonoids (N=56)

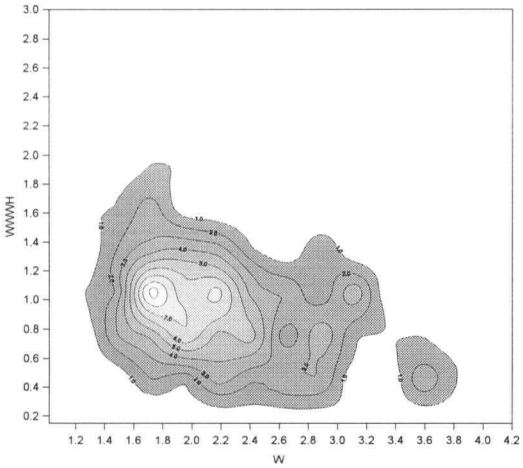

Figure 3-17 W-WWWH contoured density for Carnian ammonoids (N=113)

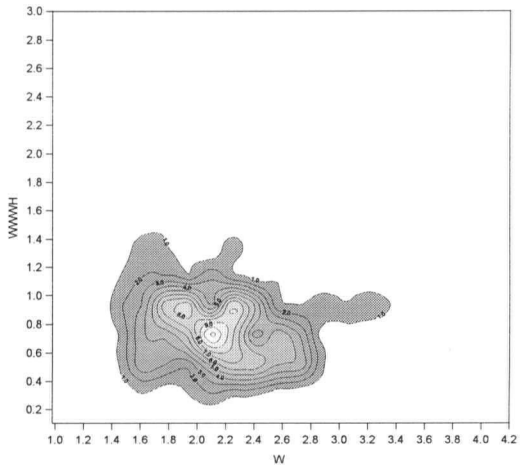

Figure 3-18 W-WWWH contoured density for Norian ammonoids (N=170)

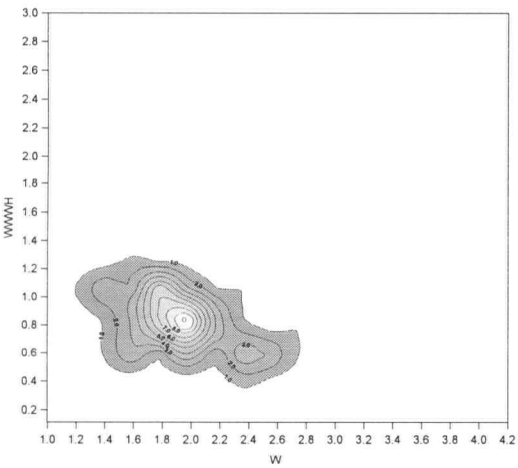

Figure 3-19 W-WWWH contoured density for Hettangian ammonoids (N=69)

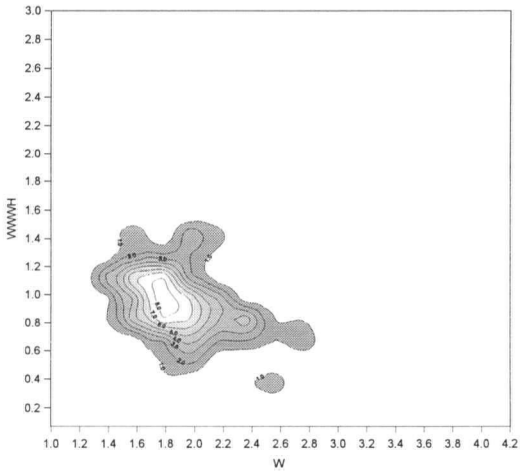

Figure 3-20 W-WWWH contoured density for Sinemurian ammonoids (N=116)

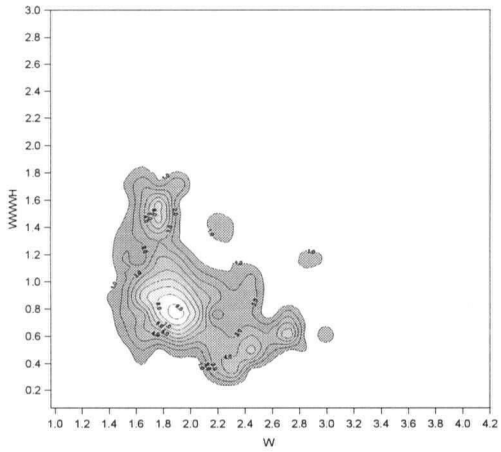

Figure 3-21 W-WWWH contoured density for Pliensbachian ammonoids (N=249)

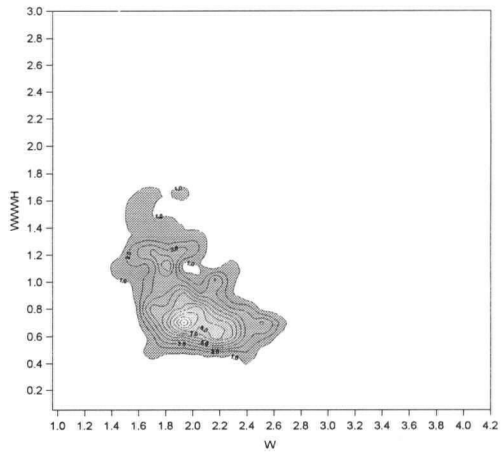

Figure 3-22 W-WWWH contoured density for Toarcian ammonoids (N=251)

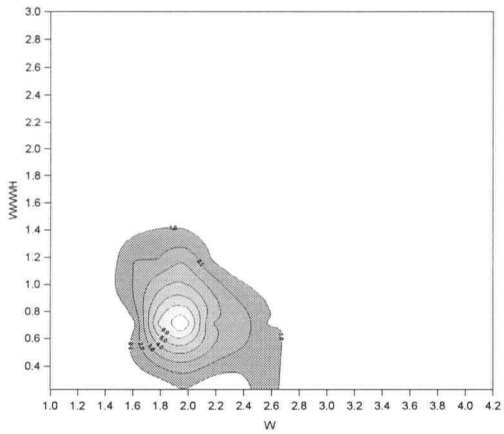

Figure 3-23 W-WWWH contoured density for Aalenian ammonoids (N=35)

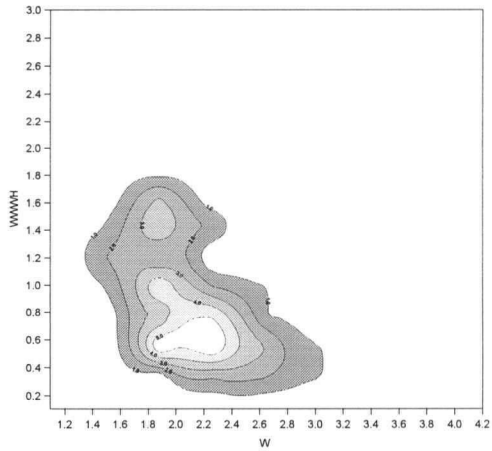

Figure 3-24 W-WWWH contoured density for Bajocian ammonoids (N=56)

3.6 Covariations of WWWH, W and U within Superfamily

In previous sections of this chapter, the morphological covariations between whorl shape (WWWH) and basic geometry of coiled shells (whorl expansion W and umbilical ratio U) have been discussed at stage level but without considering taxonomic effects. The superfamily in Triassic ammonoids has long been used as the principal high level taxon. In the following section, I will try to demonstrate the covariations between whorl shape and basic shell geometry to the two major superfamilies of Upper Triassic Norian Stage. The samples with available W, U, and WWWH data belonging to two superfamilies (Nathorstitaceae, Tropitaceae) in the Norian Stage have been selected. Within each superfamily, the samples were nearly evenly divided into three groups respectively according to the ranges of W and U values, and then each group's average values of W, U, and WWWH were calculated. So the changes in the WWWH value can be viewed according to the increase of W and U values.

Nathorstitaceae: 120 specimens are selected from this superfamily. The specimens are evenly divided into three groups based on the range of W values (Table 3-1) and the range of U values (Table 3-2).

	W (< 2.2)	U	WWWH
Average	1.87	0.30	0.90
Standard Deviation	0.20	0.13	0.26
	W (2.2 - 2.5)	U	WWWH
Average	2.32	0.25	0.82
Standard Deviation	0.09	0.13	0.28
	W (> 2.5)	U	WWWH
Average	2.97	0.20	0.68
Standard Deviation	0.43	0.13	0.26

Table 3-1 The average values for W, U, and WWWH of Nathorstitaceae samples in three different W range groups

Table 3-1 shows that in three groups, when the average value of W increases, the average value of WWWH decreases.

	W	U (< 1.5)	WWWH
Average	2.69	0.10	0.58
Standard Deviation	0.58	0.03	0.17
	W	U (0.15 - 0.32)	WWWH
Average	2.36	0.23	0.75
Standard Deviation	0.43	0.05	0.20
	W	U (> 0.32)	WWWH
Average	2.23	0.40	1.04
Standard Deviation	0.48	0.05	0.25

Table 3-2 The average values for W, U, and WWWH of Nathorstitaceae samples in three different U range groups

Table 3-2 shows that in three groups, when the average value of U increases, the average value of WWWH increases.

Tropitaceae: 169 specimens are selected from this superfamily. The specimens are evenly divided into three groups based on the range of W values (Table 3-3) and the range of U values (Table 3-4).

	W (< 1.8)	U	WWWH
Average	1.56	0.19	0.88
Standard Deviation	0.16	0.14	0.29
	W (1.8 - 2.2)	U	WWWH
Average	2.01	0.18	0.80
Standard Deviation	0.10	0.12	0.18
	W (> 2.2)	U	WWWH
Average	2.55	0.16	0.79
Standard Deviation	0.33	0.11	0.25

Table 3-3 The average values for W, U, and WWWH of Tropitaceae samples in three different W range groups

Table 3-3 shows that in three groups, when the average value of W increases, the average value of WWWH decreases.

	W	U(< 0.10)	WWWH
Average	2.12	0.07	0.72
Standard Deviation	0.55	0.02	0.16
	W	U (0.11 - 0.20)	WWWH
Average	2.10	0.12	0.77
Standard Deviation	0.48	0.01	0.19
	W	U (> 0.20)	WWWH
Average	1.96	0.33	0.98
Standard Deviation	0.39	0.09	0.30

Table 3-4 The average values for W, U, and WWWH of Tropitaceae samples in three different U range groups

Table 3-4 shows that in three groups, when the average value of U increases, the average value of WWWH increases.

3.7 Discussion

As mentioned in Chapter 2, "Buckman's law of covariation" describes correlations among shell geometries and shell ornamentation. Westermann (1966) also observed an apparently significant positive correlation of whorl shape (WWWH) against relative umbilical width (U). The narrower the umbilicus, the more compressed the whorl will be.

Raup (1967) plotted the average WWWH data for natural occurrences of 405 Phanerozoic planispiral ammonoid genera selected from Treatise (Arkell et al., 1957) on a W-U coordinate system (Figure 3-25). The figure shows that WWWH increases toward the high U – low W region.

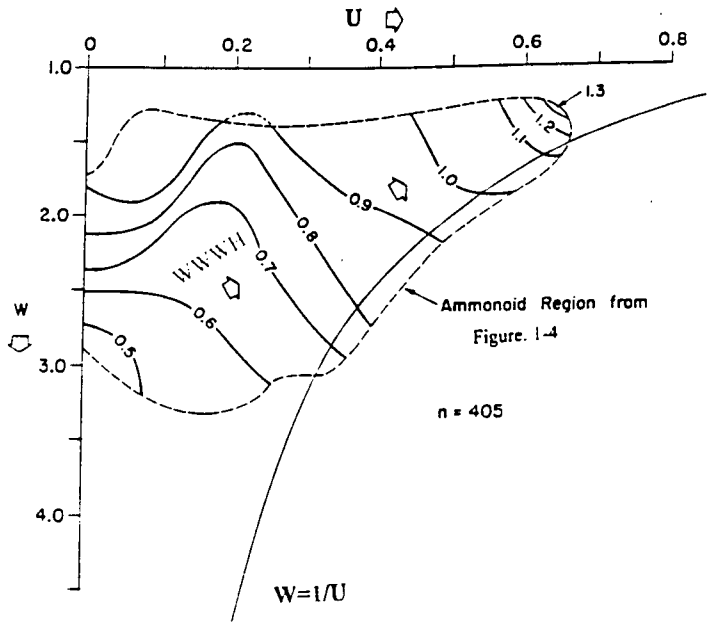

Figure 3-25 Variation in average WWWH with respect to W and U for Phanerozoic ammonoids (Raup, 1967)

Raup (1967) also created a contoured U - WWWH density map (Figure 3-26). It is obvious that WWWH is strongly correlated with U. When U increases, so does

WWWH. Although the distribution of WWWH with respect to W was not shown, Raup (1967) concluded that the correlation between these two parameters is apparently negative.

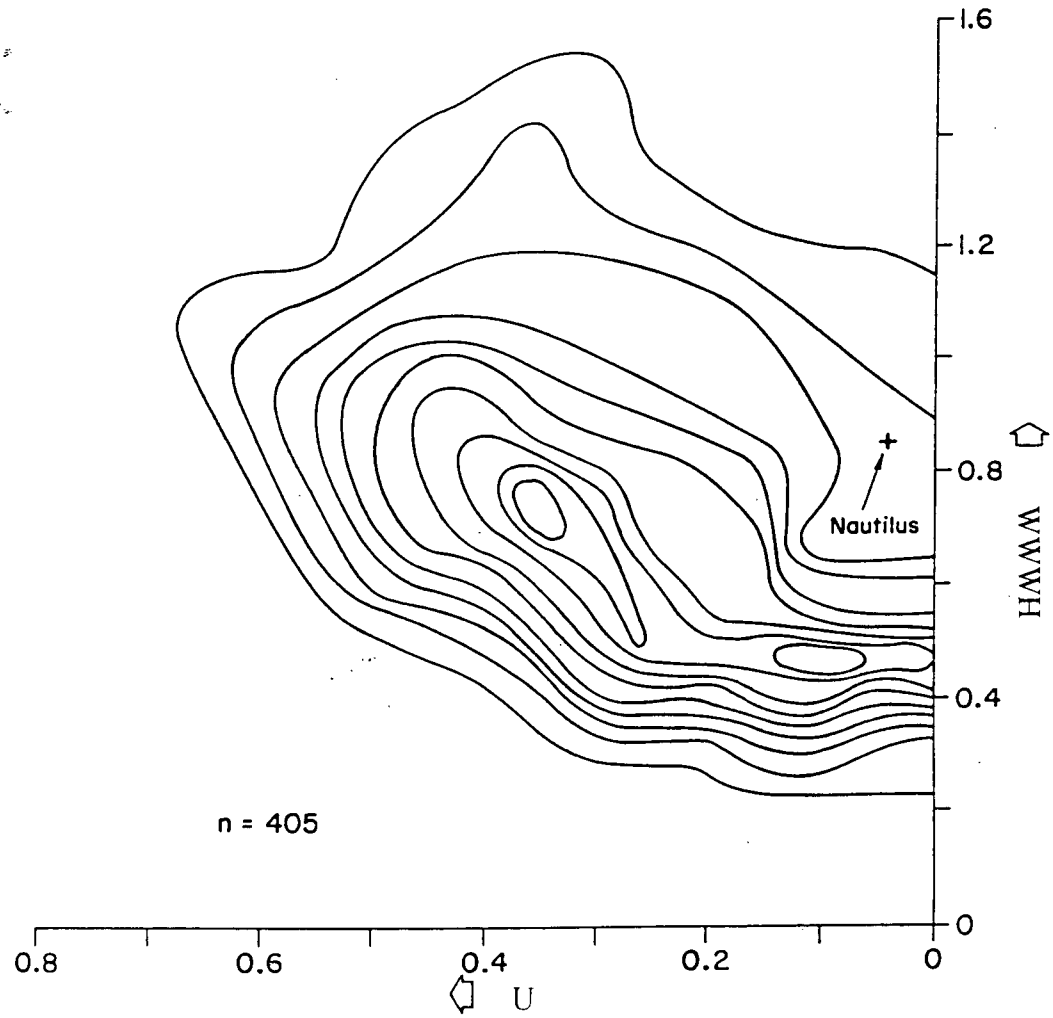

Figure 3-26 Contoured density (with respect to U and WWWH) of natural occurrence of planispiral ammonoids (Raup, 1967)

By using the data of whole samples stored in the AMMON database, Liang (1994) created a WWWH contoured density map with respect to W and U (Figure 3-27).

The map shows that the lowest WWWH density value locates at high W (W=2.4) and low U area (U=0). When W increases, WWWH decreases. So the correlation between WWWH and W is negative.

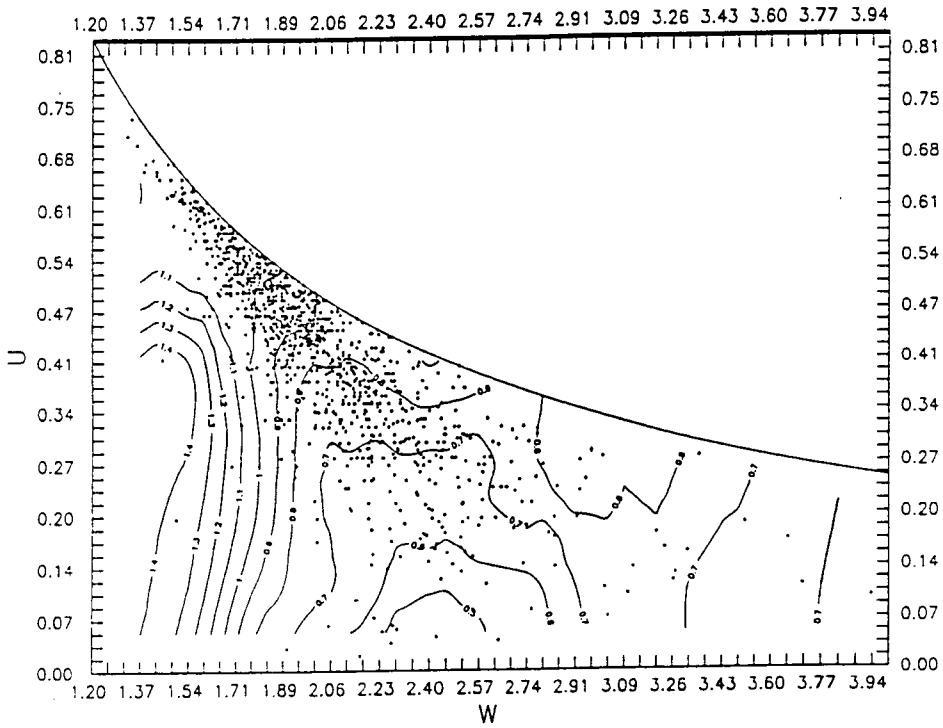

Figure 3-27 WWWH contoured density with respect to W and U (whole sample from AMMON) (Liang, 1994)

In the research presented here, the contoured WWWH density maps (Figure 3-1 to Figure 3-8) with respect to W and U basically show the similar results as Raup (1967) and Liang (1994). The highest WWWH densities are generally located at low W areas, like the Late Triassic Carnian (Figure 3-1) and Norian stages (Figure 3-2), the Early Jurassic Toarcian Stage (Figure 3-6), or are located at high U regions, like the Early Jurassic Hettangian Stage (Figure 3-3), Sinemurian Stage (Figure 3-4), Pliensbachian

Stage (Figure 3-5), and the Middle Jurassic Aalenian Stage (Figure 3-7). For some stages, like the Bajocian (Figure 3-8), extra high WWWH density distributes at relatively high W and low U areas.

The result of U-WWWH contoured densities (Figure 3-9 to Figure 3-16) generally display positive correlations between U and WWWH. In the Late Triassic Carnian and Norian stages, the contoured diagrams show broad and multi-peaked patterns, and the weak U-WWWH positive correlations. For the stages of Early and Middle Jurassic, the positive correlations are much more obvious. However, in the areas with relatively high WWWH value, when WWWH>1.2 in the Early Jurassic, and when WWWH>0.8 in the Middle Jurassic, the U-WWWH positive correlations do not exist. When WWWH increases, the U value does not change.

The W-WWWH contoured density maps (Figure 3-17 to Figure 3-24) show negative correlations between W and WWWH. In the Carnian and Norian stages the negative correlation is very weak due to the broad contour patterns. In the stages of the Early and Middle Jurassic, the negative correlations of W and WWWH become apparent. In relatively high WWWH areas (basically when WWWH>1.2), the W-WWWH negative correlation does not exist. When WWWH increases, W does not decrease.

Based on the ranges of W and U values, separately dividing the samples belonging to two Norian Stage superfamilies, Nathorstitaceae and Tropitaceae, shows the negative correlation between W and WWWH, and positive correlation between U and WWWH (Table 3-1 to Table 3-4).

I contoured the W and U data respectively belonging to these two superfamilies (Figures 3-27 and 3-28). The contoured W and U diagram for Nathorstitaceae clearer

linear pattern and its high peak has much larger U values than that of Trotitaceae. It is possible that this implies Nathorstitaceae is the rootstock for the Jurassic ammonoids.

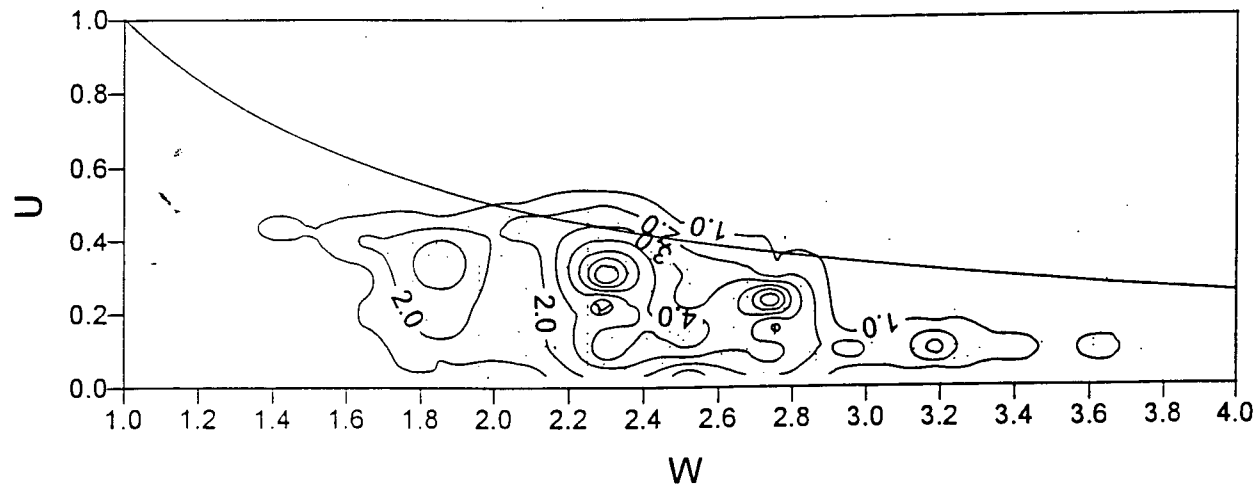

Figure 3-27 Contoured W-U density diagram for Nathorstitaceae (N=122)

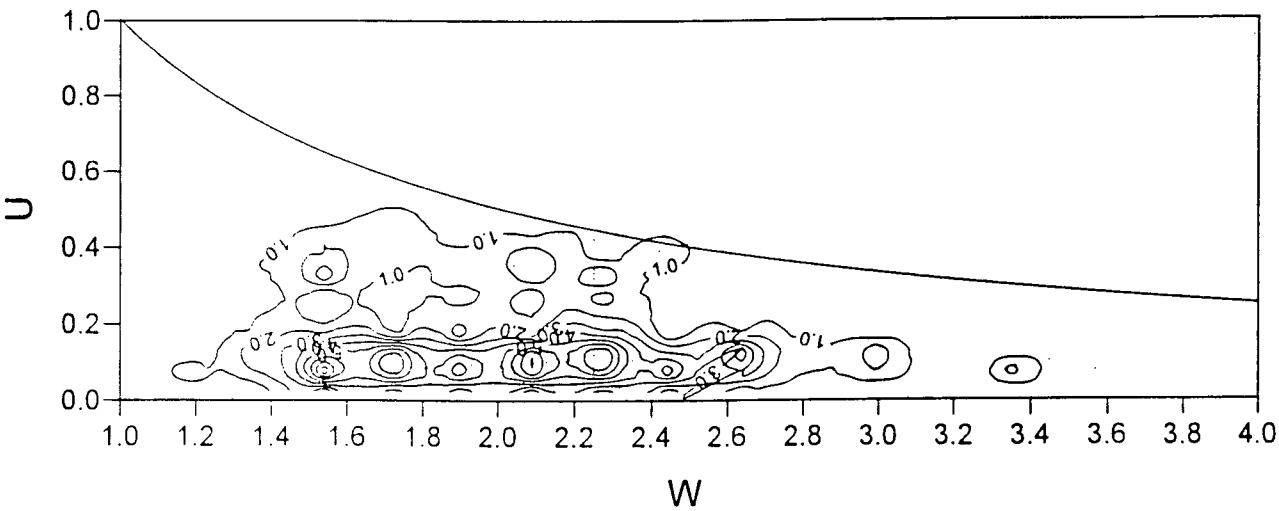

Figure 3-28 Contoured W-U density diagram for Tropitaceae (N=178)

Chapter 4 Ammonoid Hydrodynamic Drag Coefficient Analysis

4.1 Introduction

As introduced in Chapter 1, drag is generated to resist an object's motion when this object moves through a fluid. The Drag coefficient (C_D) can be used to describe the drag producing capacity of a particular shape and can be thought of as representing the hydrodynamic efficiency of an object. After a series of tests on the effect of shape on hydrodynamic efficiency, Chamberlain (1976) suggested that most of the drag caused by a cephalopod derive from a few morphologic features of the shell. They are (1) the size of the umbilicus, (2) the width of the shell relative to its diameter (fineness ratio), and (3) the size of the aperture. To explore the hydrodynamic effect of different shell geometries, Chamberlain (1980) contoured model derived C_D data based on variations in whorl expansion rate (W) and umbilical ratio (U) for smooth models with circular whorl section (WWWH=1). Two points of low C_D fell within this region. Their positions are at W=1.5, U=0.1 and the other at W=2, U=0.43 (Figure 1-4). These two points mark the geometries with the lowest C_Ds and the highest hydrodynamic efficiencies.

In this chapter, the W-U density contoured maps and 3-D diagrams of equidimensional whorl shape ammonoids are created from the Upper Triassic Carnian Stage through the Middle Jurassic Bajocian Stage. Low C_D values are plotted on these contoured maps and 3-D diagrams. The hydrodynamic efficiency of ammonoids within these stages is then discussed.

4.2 Data and Sampling

The major data sources for this research are from the AMMON database, Tozer (1994), Arkell et al. (1957), Wiedmann (1973), Taylor (1988), etc. A set of specimens were selected with equidimensional whorl cross sections from the Upper Triassic Carnian Stage through the Middle Jurassic Bajocian Stage. The range of WWWH values is 0.9-1.1 for the Carnian Stage through the Toarcian Stage. Due to the limited number of specimens in the Aalenian Stage and the Bajocian Stage, the range of WWWH values is increased to 0.7-1.3 within these two stages. By comparing the highest contour peak positions of these maps and Chamberlain's low C_Ds' positions, we may gain a general impression of the ammonites' moving efficiency through these stages and the correlation between shell geometry and hydrodynamic efficiencies.

4.3 Geometry through Time

Based on the selected data, W-U density contoured maps and their relevant 3-D diagrams (Figure 4-1 to Figure 4-16) were created for the Upper Triassic Carnian Stage through the Middle Jurassic Bajocian Stage. The W=1/U offlap line is overlaid on these maps and the 3-D diagrams.

Carnian Stage: 70 specimens with equidimensional whorl cross sections are used to create the W-U density contoured map. The geometry displays in a broad, nonlinear pattern. Two low C_D points are within the contoured area. There are multi-peaks appeared. The position of the peak having the highest contour value is at W=2.5 and U=0.15 (Figure 4-1 and Figure 4-9).

Norian Stage: 118 equidimensional whorl specimens are selected. The geometry displays a similar pattern as the Carnian Stage: broad and nonlinear. The contoured region covers two low C_D points. The highest contour peak is at W=2.3 and U=0.33 (Figure 4-2 and Figure 4-10).

Hettangian Stage: The W-U density contoured map is made based on 66 selected equidimensional whorl samples. The map shows a narrow and linear pattern along the offlap line and distributes at relatively low W and high U area. Two peaks are within the region. The higher peak is at W=1.83 and U=0.46 which is near one of the low C_D postion. The lower peak is at W=1.41 and U=0.63 (Figure 4-3 and Figure 4-11).

Sinemurian Stage: 189 equidimensional whorl specimens are selected. The W-U density contoured map has the similar geometric pattern with the Hettangian Stage: narrow and linear distribution at the low W and high U area. There are two obvious peaks. The position of the higher peak is at W=1.85 and U=0.47; the lower one is at W=2.05 and U=0.41 (Figure 4-4 and Figure 4-12).

Pliensbachian Stage: 256 equidimensional whorl specimens are chosen. The highest W-U contoured density peak is located at W=1.78 and U=0.5 (Figure 4-5 and Figure 4-13).

Toarcian Stage: There are 225 equidimensional whorl specimens selected. The highest W-U contoured density peak is at W=1.82, U=0.5 (Figure 4-6 and Figure 4-14).

Aalenian Stage: 60 equidimensional whorl specimens are selected. Comparing the W-U density contoured maps for the Lower Jurassic stages, the geometry of the W-U density contoured map in this stage has a relatively broad pattern, and distributed at

relatively high W and low U area. The density peak is located at W=1.88, U=0.47 (Figure 4-7 and Figure 4-15).

Bajocian Stage: 42 equidimensional whorl specimens are selected. The pattern of the W-U density contoured map is similar with the Aalenian Stage, but the geometry distributes at the two sides of offlap line due to the existence of heteromorph ammonoids. The density peak is located at W=1.91 and U=0.38 (Figure 4-8 and Figure 4-16).

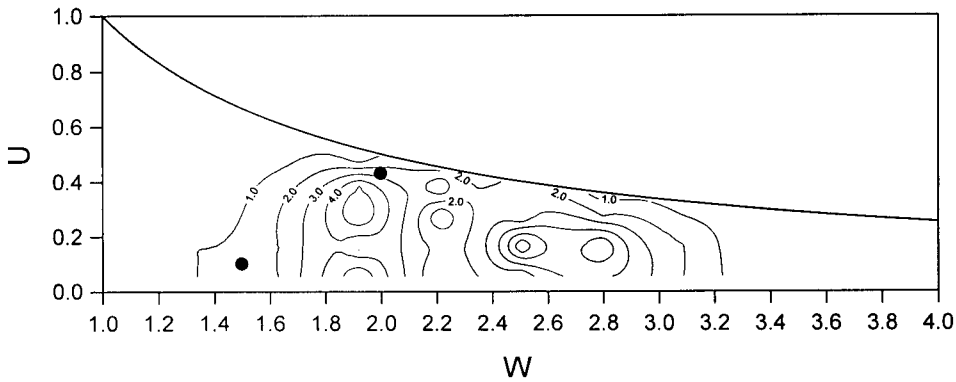

Figure 4-1 Contoured density diagram for Carnian ammonoids. Black dots mark the low C_D positions (N=70)

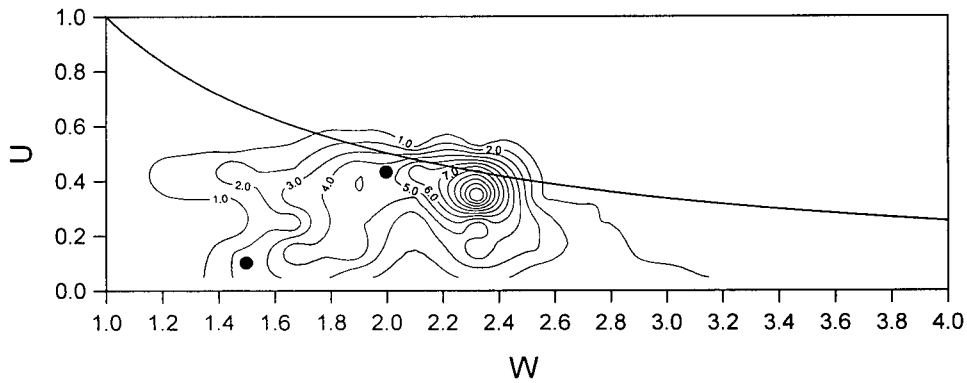

Figure 4-2 Contoured density diagram for Norian ammonoids. Black dots mark the low C_D positions (N=118)

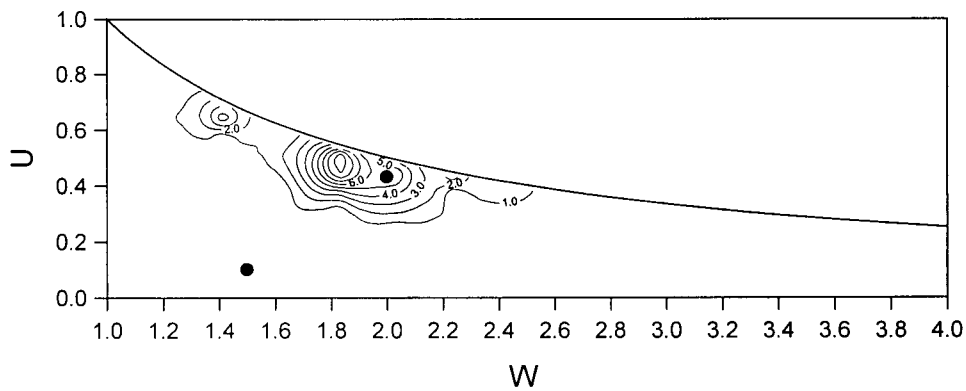

Figure 4-3 Contoured density diagram for Hettangian ammonoids. Black dots mark the low C_D positions (N=51)

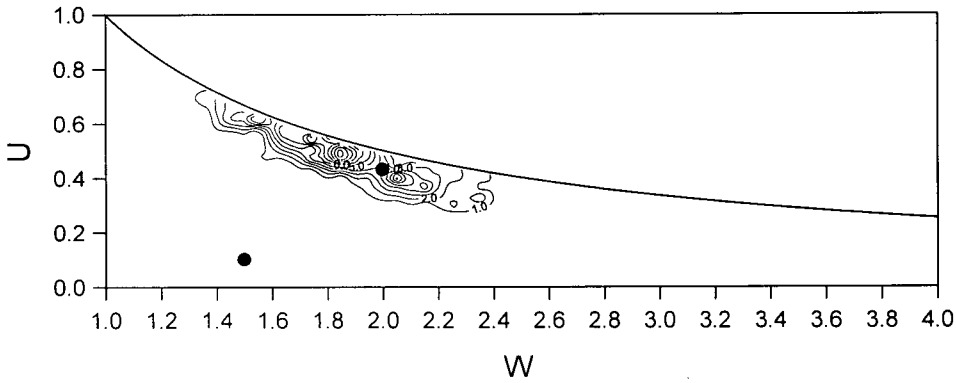

Figure 4-4 Contoured density diagram for Sinemurian ammonoids. Black dots mark the low C_D positions (N=189)

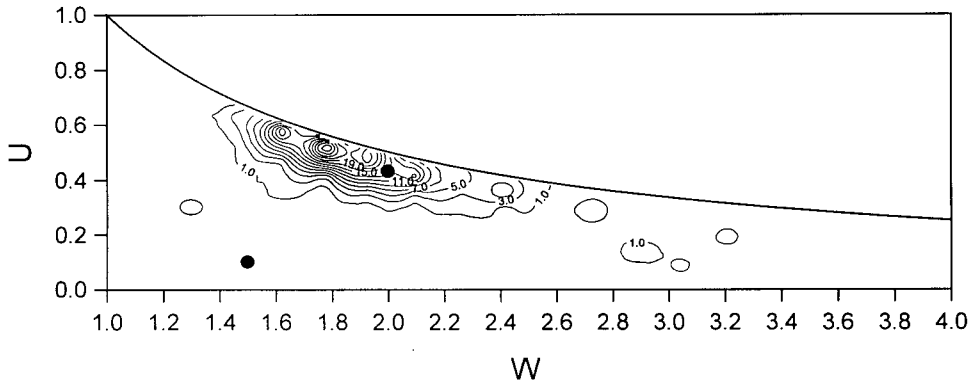

Figure 4-5 Contoured density diagram for Pliensbachian ammonoids. Black dots mark the low C_D positions (N=256)

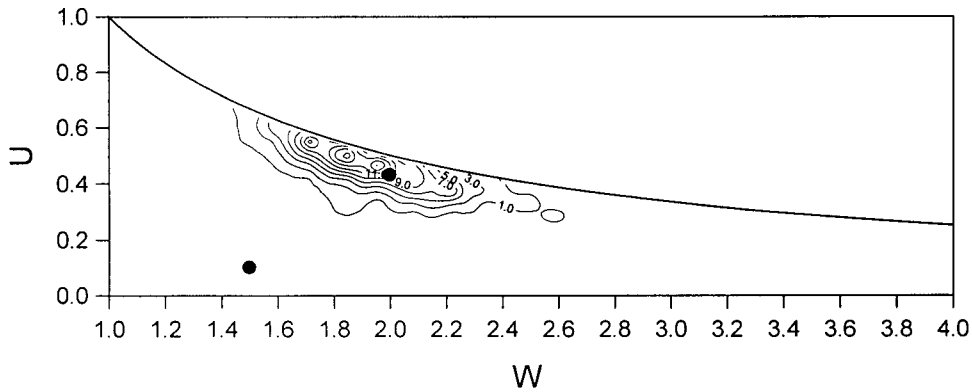

Figure 4-6 Contoured density diagram for Toarcian ammonoids. Black dots mark the low C_D positions (N=225)

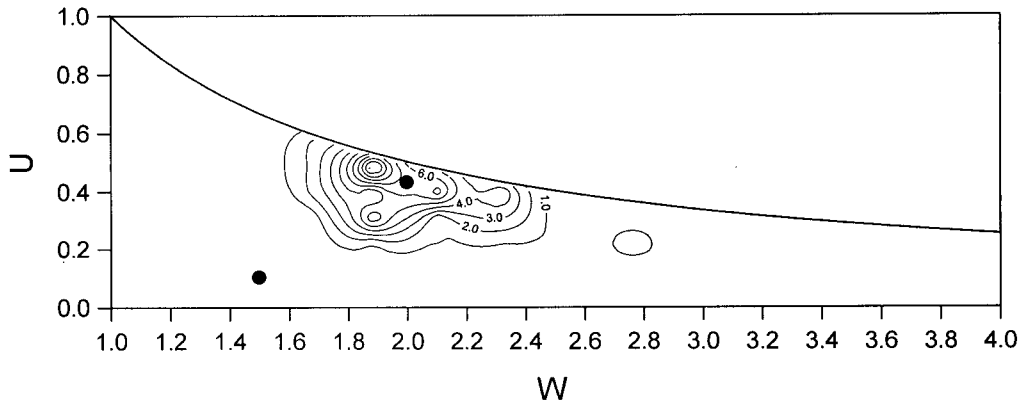

Figure 4-7 Contoured density diagram for Aalenian ammonoids. Black dots mark the low C_D positions (N=60)

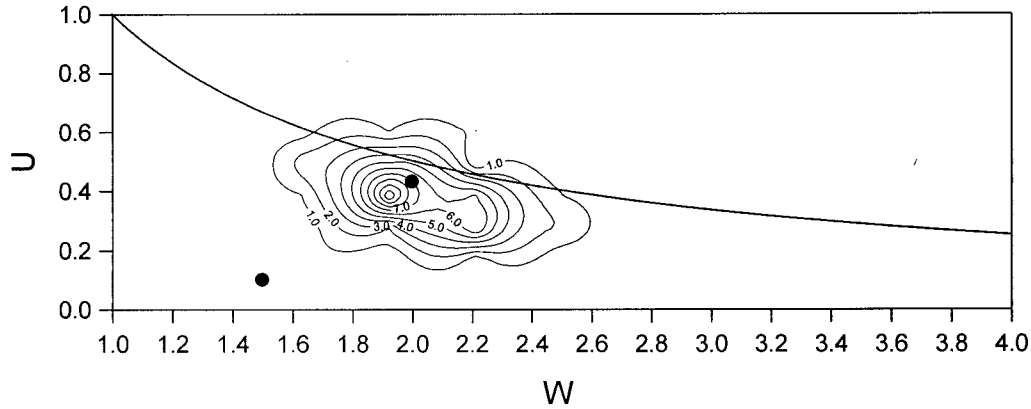

Figure 4-8 Contoured density diagram for Bajocian ammonoids. Black dots mark the low C_D positions (N=42)

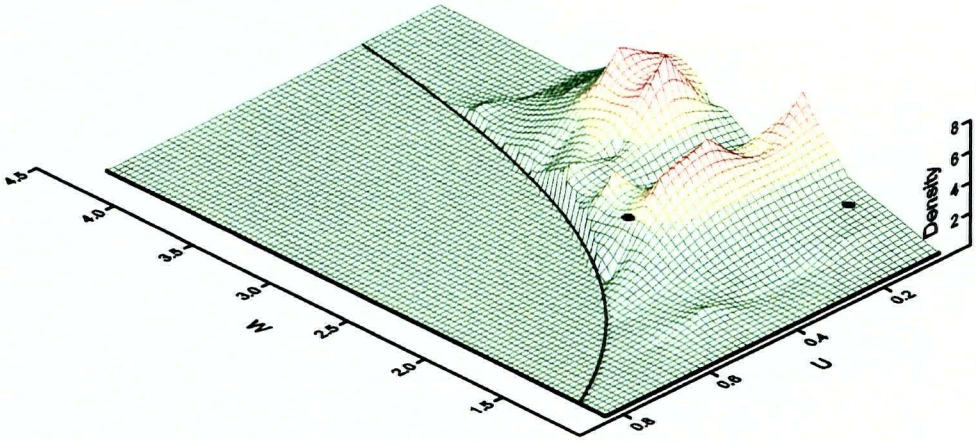

Figure 4-9 3-D density diagram for Carnian ammonoids. Black dots mark the low C_D positions (N=70)

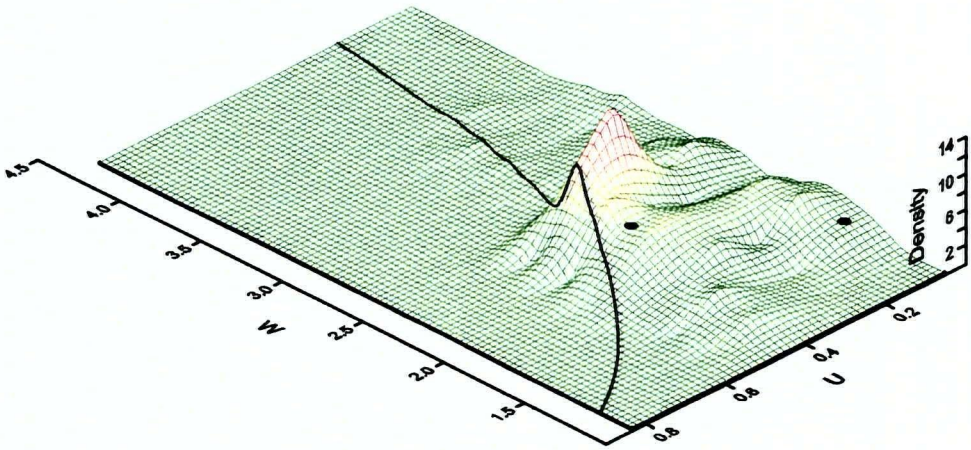

Figure 4-10 3-D density diagram for Norian ammonoids. Black dots mark the low C_D positions (N=118)

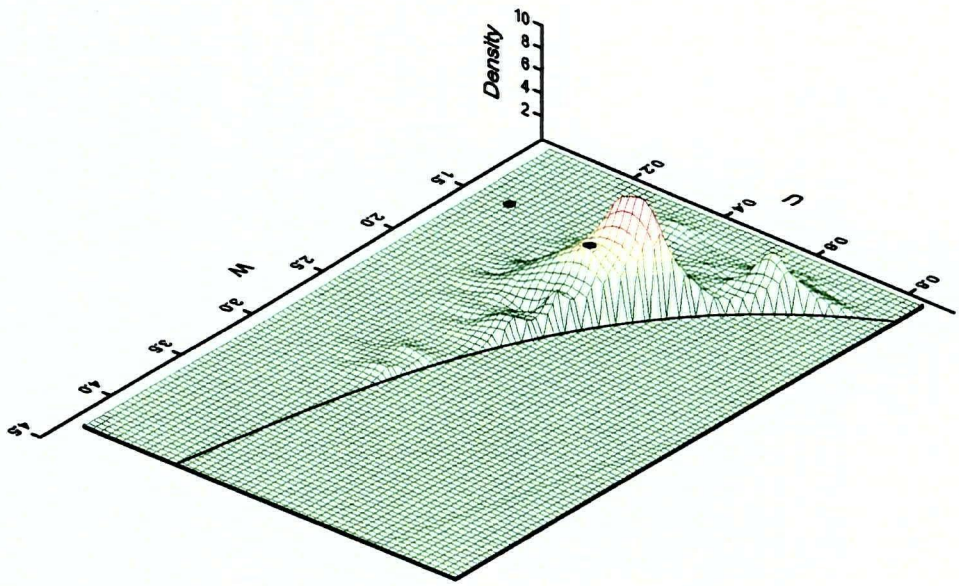

Figure 4-11 3-D density diagram for Hettangian ammonoids. Black dots mark the low C_D positions (N=51)

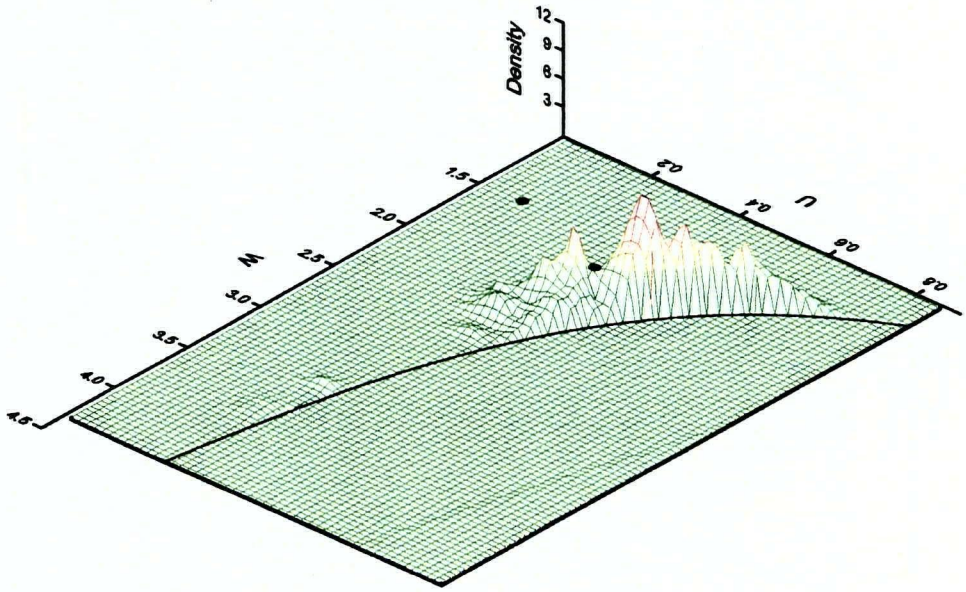

Figure 4-12 3-D density diagram for Sinemurian ammonoids. Black dots mark the low C_D positions (N=189)

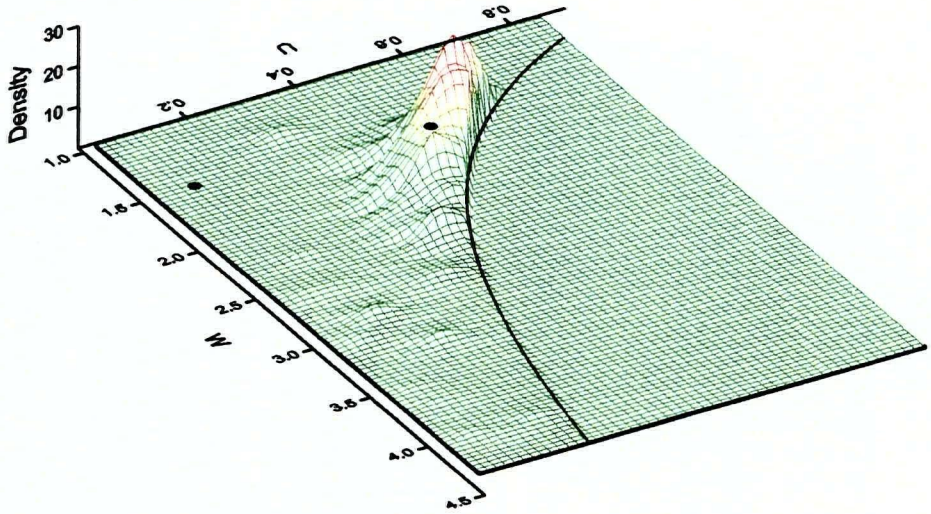

Figure 4-13 3-D density diagram for Pliensbachian ammonoids. Black dots mark the low C_D positions (N=256)

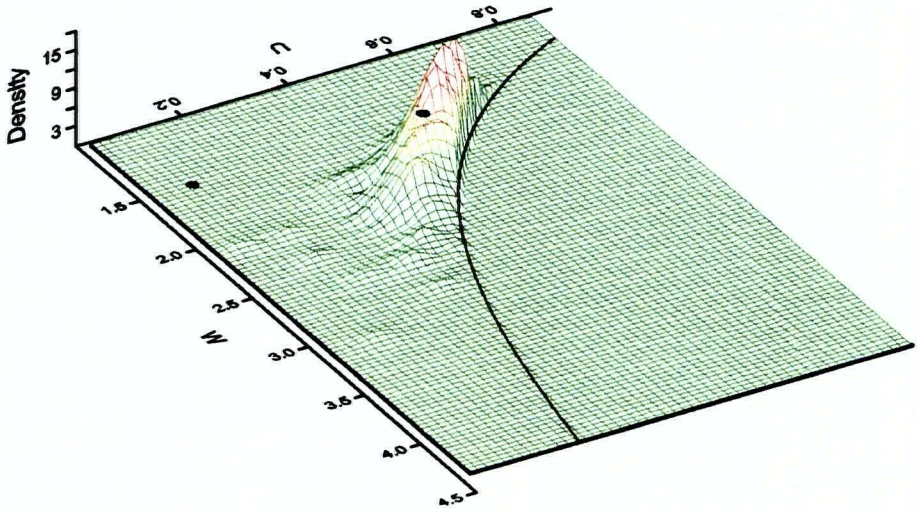

Figure 4-14 3-D density diagram for Toarcian ammonoids. Black dots mark the low C_D positions (N=225)

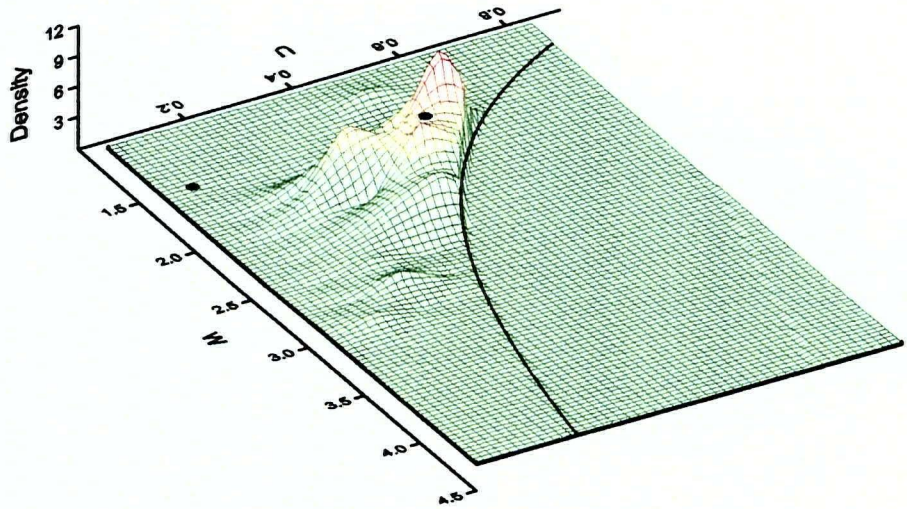

Figure 4-15 3-D density diagram for Aalenian ammonoids. Black dots mark the low C_D positions (N=60)

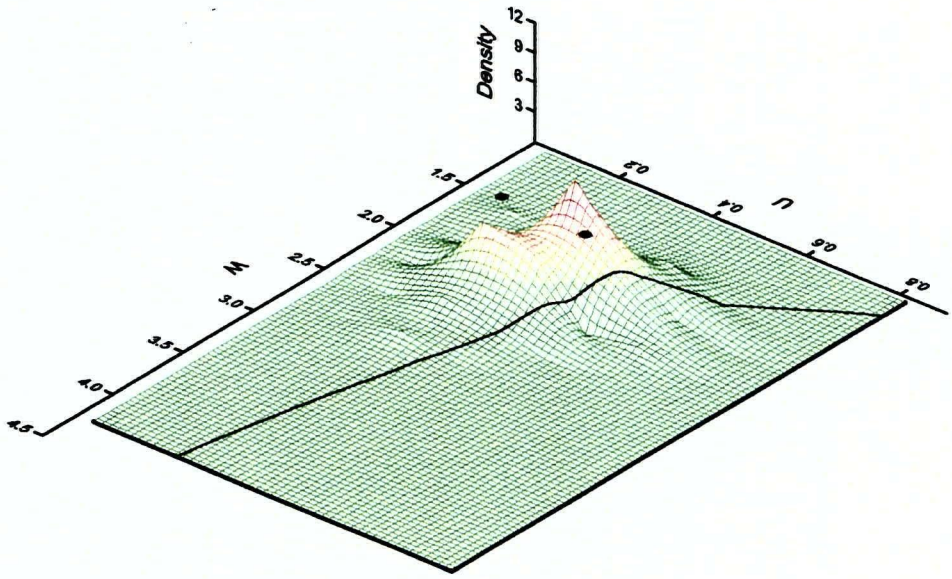

Figure 4-16 3-D density diagram for Bajocian ammonoids. Black dots mark the low C_D positions (N=42)

4.4 Discussion

Geometry density diagrams like Figure 4-1 to 4-16 can be useful in highlighting evolutionary history. By exploiting particular morphologies, the degree of the evolutionary shifts can be approached. Overlying Chamberlain's two low C_D points (1981) on the W-U contoured density diagrams and 3-D diagrams described above (Figure 4-1 to 4-16), we find that the shell geometry of the ammonoids in the four stages of Early Jurassic and the two stages of Middle Jurassic distribute at the relatively low W and high U area of the morphological spectrum. Their high peaks are in the vicinity of high U C_D point (W=2, U=0.43) reflecting hydrodynamic efficiency as determined by Chamberlain (1980). However, the ammonoid geometries in Late Triassic Carnian and Norian stages are scattered over wide regions covering both of the two low C_D points. The highest peak of the Carnian Stage W-U density contoured map is at high W value area and its position (W=2.5, U=0.15) is far from low C_D points (Figure 4-1 and Figure 4-9), which indicates that the Carnian Stage ammonites have a high whorl expanding rate but low hydrodynamic efficiency. The highest peak of the shell geometry in the Norian Stage has smaller W value (W=2.3) but bigger U value (U=0.33), which is closer to one of Chamberlain's low C_Ds points (Figure 4-2 and Figure 4-10). So the Norian Stage ammonite shells appear to be more evolute, and their efficiency is higher. Throughout the stages from Carnian to Bajocian, the ammonoids tend to have higher hydrodynamic efficiency.

Based on the ammonoid geometric data, Chamberlain (1980) produced the W-U density distribution plots according to geologic range - Paleozoic, Triassic, and Jurassic+Cretaceous (Figure 4-17). The ammonoid plots in this figure are for goniatites,

ceratites, and ammonites. The Paleozoic forms are centered in the low W and low U area where are away from C_D peaks. Eventually the shells then shift towards the high U, low

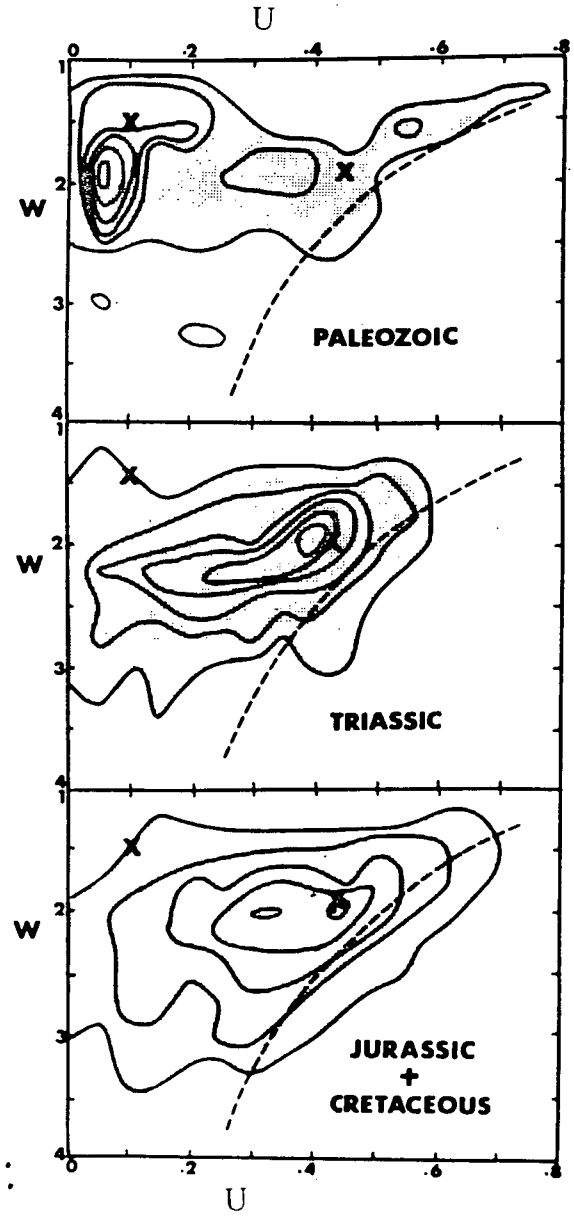

Figure 4-17 Preferred shell geometries of ammonoids through time. Positions of high hydrodynamic efficiency shown by Xs. Dashed line - offlap line (W=1/U) (Chamberlain, 1980)

C_D peak and the geometric range expands to fill the whole low C_D area. While in our W-U density diagrams, the Carnian Stage (Figure 4-1 and Figure 4-9) has a pattern similar to Chamberlain's Paleozoic figure. Both have low W peaks that are far from two C_D positions but the whole contoured range covers two low C_D points. While in the Norian Stage (Figure 4-2 and Figure 4-10), the general density pattern is close to Chamberlain's Triassic figure. The U value of the contour peak is bigger, and the distribution of the geometry is closer to the high U, low C_D peak. So Chamberlain's observation about Paleozoic forms can be applied to the Carnian Stage of the Upper Triassic.

Compared with Chamberlain's Jurassic+Cretaceous geometric figure, the similarity of our W-U density diagrams within Jurassic (Hettangian Stage to Bajocian Stage) is that the geometric plots concentrate in the vicinity of the high U, low C_D (Figures 4-3 to 4-8; Figures 4-11 to 4-16). The difference is that our diagrams do not distribute in the low U area and exclude the low U, low C_D point, but the contour range of Chamberlain's figure is much wider and the low U, low C_D point is included. The explanation for this might be that our diagrams only use roughly equidimensional section whorl shells but Chamberlain's map has wider sampling range.

The Upper Triassic through Middle Jurassic W-U density geometries basically reflect three evolution intervals discussed in Chapter 2 (pre-extinction, post-extinction, and recovery). In the Upper Triassic Carnian and Norian stages, geometries have broad, nonlinear, and multi-peaked patterns and cover two low C_D points but show low hydrodynamic efficiencies. In the Early Jurassic, W-U density diagrams show a narrow, linear, and one obvious peak geometry pattern. They have high U W-U density regions and negative correlation between W and U. The density peaks are in the vicinity of high

U C_D point which reflect the high hydrodynamic efficiencies. While in Middle Jurassic, the geometries display a broad, less obviously linear pattern, low U W-U density and weak negative W-U correlation.

Chapter 5 Analysis of Morphological Range Diversity

5.1 Introduction

"Since form represents the raw data of paleobiology, it is important to document significant events in the history of life from the standpoind of morphology" (Foote, 1991). In this chapter, I attempt to analyze the ammonoid morphological diversity at eight successive stages from Late Triassic through Middle Jurassic by accumulating the morphological ranges of some major morphological parameters. Morphological range diversity for an almost 70 million year interval can be viewed both before and after T/J boundary mass extinction period. Up until now in this thesis, the emphasis has been on shell geometry and whorl shape. In this chapter, the data are expanded to include features of the venter and ornamentation. This is a comprehensive approach to the question "how did the range of morphospace occupation change across the T/J boundary and how long the recovery take?"

5.2 Data Sampling and Choice of Characters

The study in this chapter is based at the generic level with data sources and sampling criteria being the same as those mentioned in Chapter 2. The total number of samples selected for each stage in this chapter is listed in Table 5-1.

Major describable shell geometry and ornamentation characters for species identification are chosen in attempt to comprehensively represent ammonoid morphologic diversity. The shell geometric parameters selected here include whorl expansion ratio (W), umbilical ratio (U), heteromorph ammonoid coiling type

(HETEROMORPH SHELL GEOMETRY, as described in Chapter 2: straight, curved, loose-sprial, and helicospiral), whorl shape (WWWH), as well as the appearance of ventral features (VENTER, as shown in Figure 5-1). Ornamentation includes the number of primary ribs per half whorl (PRHW), the number of tubercles per half whorl (THW), the pattern of rib furcation (FURC, as shown in Figure 5-2), and the arrangement of tubercles (TUBERC, as shown in Figure 5-3).

Stage	Number of Samples Selected
Bajocian Stage	187
Aalenian Stage	74
Toarcian Stage	300
Pliensbacian Stage	353
Sinemurian Stage	179
Hettangian Stage	121
Norian Stage	218
Carnian Stage	148

Table 5-1 The number of samples selected for each stage in the analysis of morphological range diversity

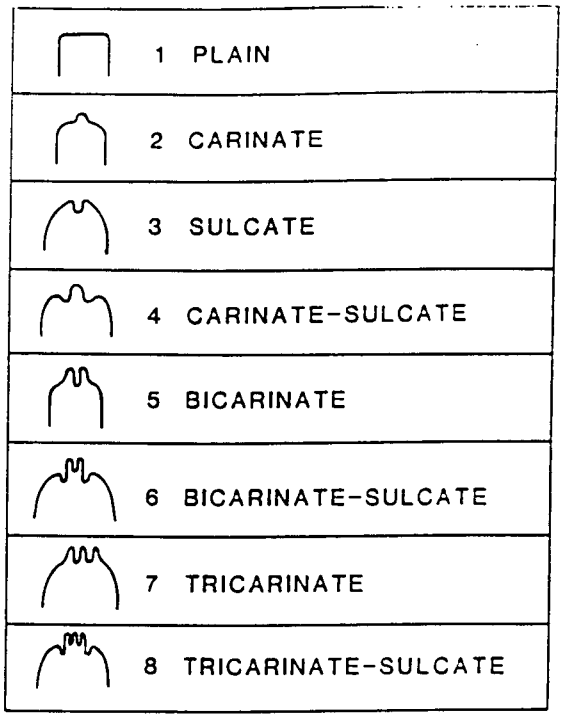

Figure 5-1 States for the descriptor VENTER (Smith, 1986)

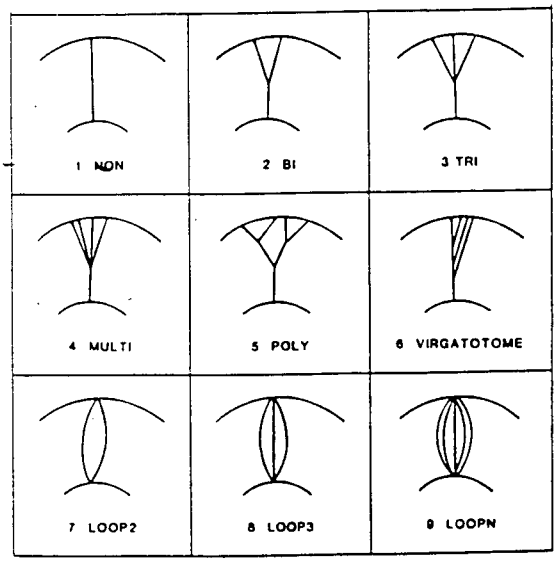

Figure 5-2 States for the descriptor FURC (Smith, 1986)

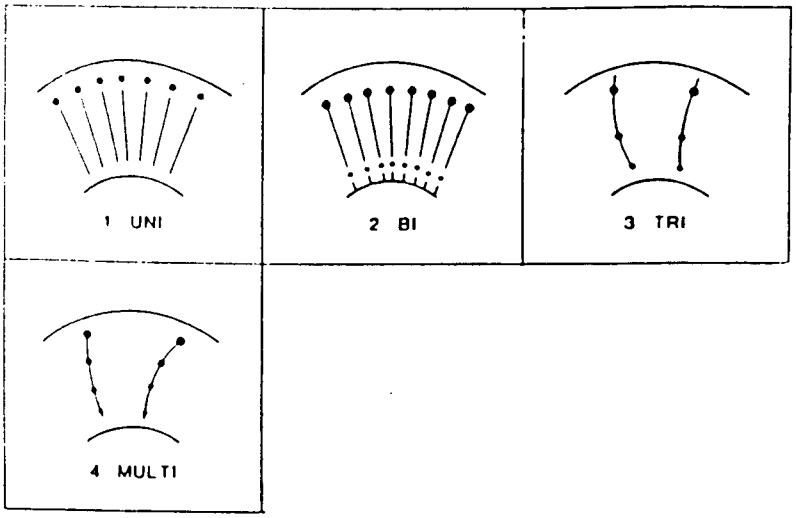

Figure 5-3 States for the descriptor TUBERC (simplified from Smith, 1986)

5.3 Morphological Range Diversity Index (MRDI)

Two types of data are used in this chapter: quantitative data and qualitative data. For the quantitative data, the variables belonging to them can be calculated, such as W, U, WWWH, PRHW, as well as THW. The qualitative data are the data having to do with qualities or states, such as VENTER, FURC, and TUBERC (Figure 5-1 to 5-3).

The MRDI for quantitative data is the difference between the maximum and minimum of the morphological characters with normalization so that the MRDI value always falls between 0 and 1, while the MRDI for qualitative data is the percentage of occupied character states (Liang, 1994).

5.4 Discussion

Figure 5-4 illustrates the morphological diversity for each of the eight stages from Late Triassic Carnian Stage through Middle Jurassic Bajocian Stage by considering the nine shell geometry and ornamentation characters. Each bar in the graph represents a

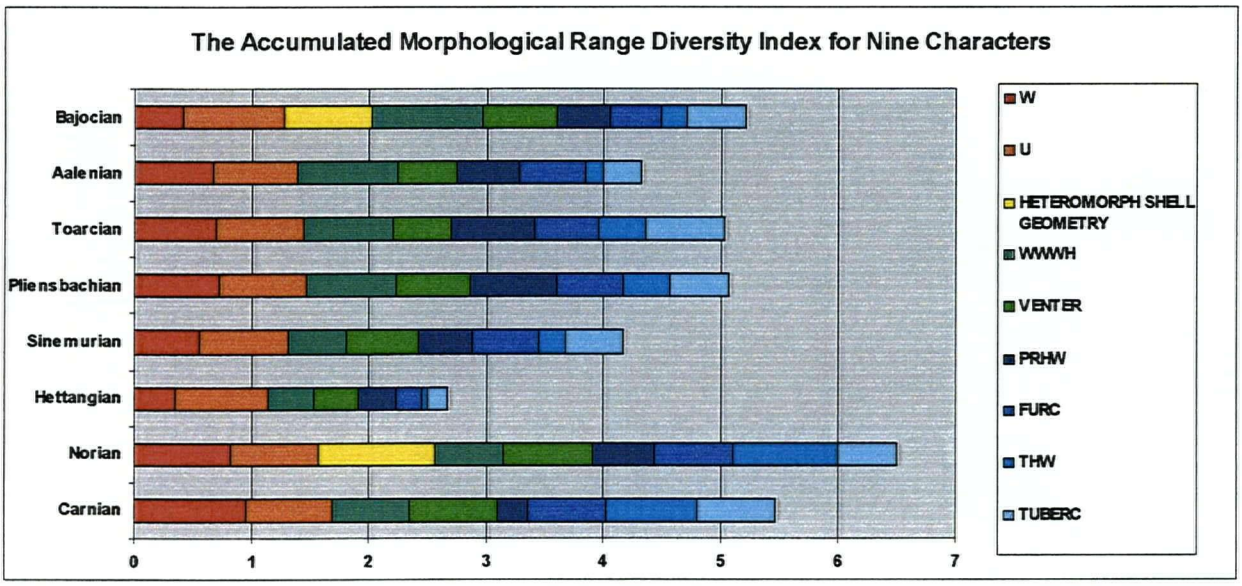

Figure 5-4 The accumulated morphological range diversity index for nine characters

stage and the morphological diversity for each character is represented by a certain color. I am interpreting this diagram in the light of our current understanding of time scale calibrations. Presumably morphological diversity takes time to accumulate and the ages are not equal units.

Based on the morphological diversity pattern (Figure 5-4), four intervals can be recognized:

1. Interval One (Carnian and Norian): This interval has a duration of 5.4 million years. The MRDI in this period is quite high and reaches its highest value in the Norian Stage due to the existence of the heteromorph ammonoids.

2. Interval Two (Hettangian and Sinemurian): The duration in this interval is 8.1 million years. After the end-Triassic mass extinction, all 46 Late Triassic families died out, and there is a dramatic fall in the MRDI during the Hettangian Stage when only a few genera belonging to Psiloceratidae, Schotheimiidae, Pleurocanthitidae, Ectocentritidae existed. The MRDI has a rapid rise in the Sinemurian Stage since most of the Psilocerataceae families had evolved by the end of this stage.

3. Interval Three (Pliensbachian and Toarcian): This interval has duration of 13.3 million years. The MRDI keeps rising in this interval because of the rapid development of families belonging to Eoderocerataceae, Dactylioceratidae, and Hildocerataceae.

4. Interval Four (Aalenian and Bajocian): This interval lasts 12.0 million years. The MRDI falls in the Aalenian possibly because of the disappearance of the Dactylioceratidae. This is a group of mostly evolute, strongly ribbed and tuberculate ammonites with plain venters. Consequently the Aalenian has almost the same MRDI as the Toarcian in shell geometry (W, U, and WWWH) and VENTER but much lower MRDI in ornamentation (PRHW, FURC, THW, TUBERC). The MRDI in the Bajocian rises greatly due to the recovery of the heteromorph group and the explosive development of Stephanocerataceae, Perispinctaceae, and Haploceratacea.

Table 5-1 lists the MRDI, duration, and the rate of morphological diversification (MRDI/Duration, each result is multiplied by ten in order to highlight the differences) for

each stage. Figure 5-5 displays the MRDI and the rate of morphological diversification (MRDI/Duration).

Stage	MRDI	Duration (Ma)	MRDI/Ma (×10)
Bajocian	5.21	8.00	6.51
Aalenian	4.32	4.00	10.80
Toarcian	5.03	5.60	8.98
Pliensbachian	5.06	7.70	6.57
Sinemurian	4.17	5.00	8.34
Hettangian	2.67	3.10	8.61
Norian	6.5	23.80	2.73
Carnian	5.46	11.60	4.71

Table 5-1 The MRDI, duration, and the rate of morphological diversification (MRDI/duration) for each stage

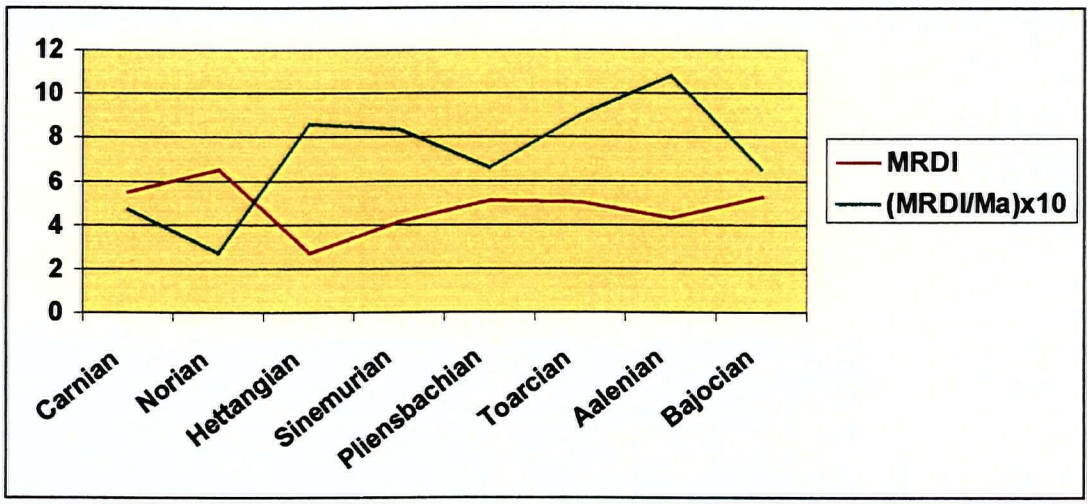

Figure 5-5 The MRDI and the rate of morphological diversification (MRDI/duration) for each stage

It appears that the correlation between duration and the rate of morphological diversification is negative. If a stage has a long duration, the rate of morphological diversification is low. On the contrary, the stage with short duration has high rate of morphological diversification. Both Carnian and Norian have low rates of morphological diversification. Major increase in rate of morphological diversification is seen in the Hettangian, which presumes that the surviving ammonoid group radiates into the niches vacated by the end-Triassic extinction.

Chapter 6 Correlation between Upper Triassic Ammonoid Suture Types and Shell Geometry

6.1 Introduction

The suture line is the line of contact between the septa and the inside of the shell. It is only visible when the shell is absent or removed. The major backward (adapical) inflections are called as lobes, and forward (adoral) inflections are called saddles. The basic components of the suture line are illustred in Figure 6-1.

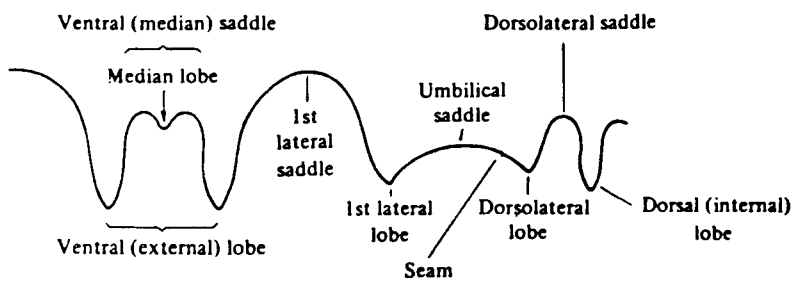

Figure 6-1 Components of the suture line (Lehmann, 1981)

Three basic types of ammonite suture are recognized during Triassic and Jurassic. They are (Figure 6-2):

(1) Goniatitic suture: having all the lobes and saddles plain, without frilling (entire, not denticulate).

(2) Ceratitic suture: having the saddles entire but the lobes denticulate.

(3) Ammonitic suture: having all the elements denticulate.

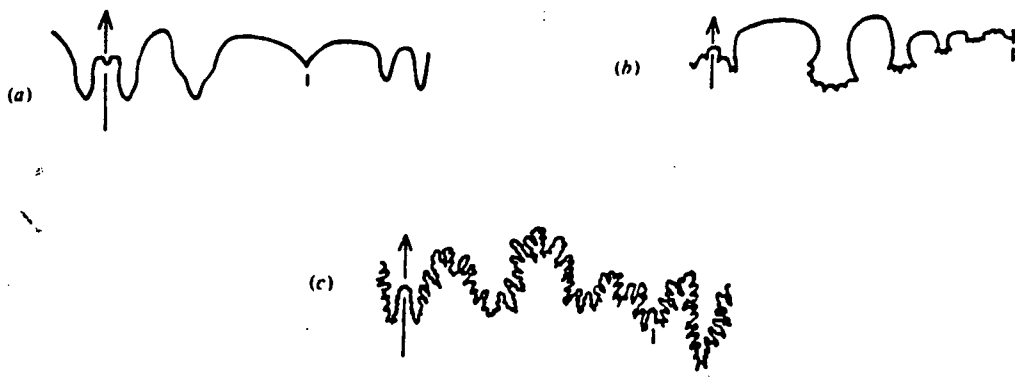

Figure 6-2 (a) Goniatitic; (b) ceratitic; and (c) ammonitic suture lines. (Lehmann, 1981)

In this chapter, the possible correlation between Late Triassic ammonoid geometry and suture type is explored. This is a significant question, because in the Hettangian Stage there is a greatly reduced spectrum of shell geometry and only one suture type (ammonitic suture).

6.2 Suture Type and Shell Geometry

Data analyzed in this chapter are taken from specimens illustrated by Tozer (1994), Arkell et al. (1957), Rakús (1993), Wiedmann (1973). The sampling criteria in this chapter are the same as in chapter 2. The sampling is based at the generic level. At most eleven species are selected within on genus, including the type species (if it is available). Only one specimen is selected for each species. Priority is given to the holotype, or to specimens that are well preserved or large. In addition, only the species for which illustrated septal suture lines are available are used in this chapter.

Based on this sampling method, in the Carnian Stage, a total of 38 specimens representing 38 species of 29 genera are selected. In the Clydonitaceae, there are 13 species belonging to 8 genera. Among these 13 species, two have goniatitic sutures, six have ceratitic sutures, and five have ammonitic sutures. In the Tropitaceae, 20 species belonging to 16 genera are selected. Two have goniatitic sutures, two have ceratitic sutures, and 16 have ammonitic sutures. Other superfamilies have relatively fewer samples. The Ceratitaceae is represented by four species (two goniatitic sutures, two ammonitic sutures). The Choristoceratacera has only one species that has a goniatitic suture. The Phylloceratacea has four species all with ammonitic sutures.

In the Norian Stage, there are a total of 113 specimens representing 113 species of 78 genera. The Nathorstitaceae has 49 species belonging to 33 genera (nine species have goniatic sutures, nineteen have ceratitic sutures, and the rest have ammonitic sutures). The Tropitaceae has 49 species belonging to 34 genera (eight have goniatitic sutures, fifteen have ceratitic sutures, and twenty-six have ammonitic sutures). Concerning other superfamilies, the Megaphyllitaceae has only one specimen selected with an ammonitic suture. The Pinacoceratacea has three specimens (all have ammonitic sutures). The Choristoceratacea has five species with goniatitic sutures. The Ussuritaceae is represented by six species all with ammonitic sutures.

With respect to the Carnian Stage and the Norian Stage, the W and U data for each selected specimen on W-U coordinate systems are represented by different shapes and colors to indicate different sutures. Yellow circles represent goniatitic sutures; green triangles represent ceratitic sutures; and red rhombus symbols represent ammonitic

sutures. As well, the W and U data of each superfamily specimens on the W-U coordinate system are plotted (Figure 6-3 to Figure 6-10).

6.3 Contoured W-U Density Diagrams

Contoured W-U density diagrams for Carnian and Norian ammonoids with different types of sutures are respectively constructed. Figure 6-11 is the contoured W-U density diagram for Carnian and Norian ammonoids having goniatitic sutures. The contour lines distribute on the two sides of offlap line (W=1/U) due to the existence of heteromorph ammonoids. The highest density peak is at the position of U=4.8 and W=2.0. Figure 6-12 displays the W-U density for those Carnian and Norian ammonoids with the ceratitic sutures. The position of the highest density peak is at U=0.33 and W=2.2. Figure 6-13 is the contoured W-U density diagram for Carnian and Norian ammonoids which have ammonitic sutures. The position of the highest density peak is at W=2.4 and the U value almost zero.

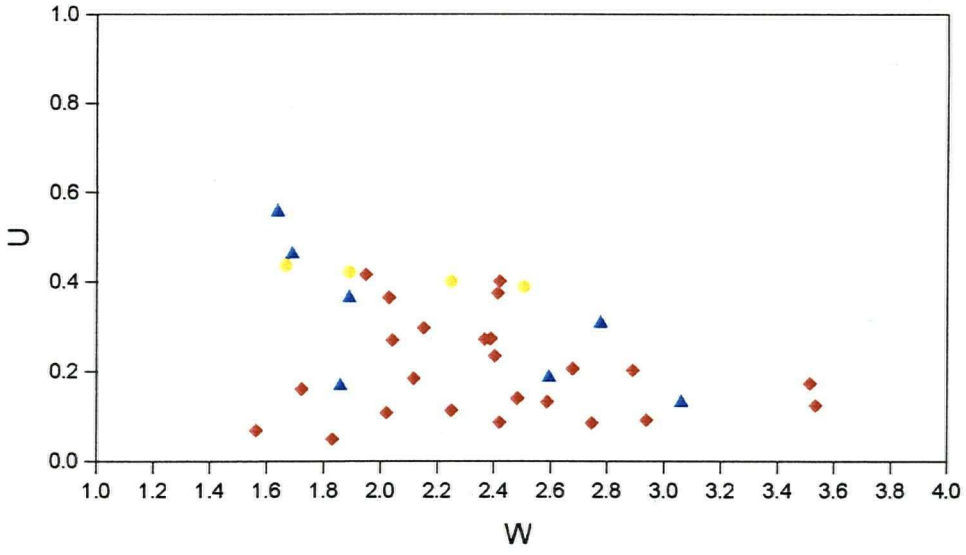

Figure 6-3 Carnian Stage ammonoids W and U data (Yellow circles: goniatitic sutures; green triangles: ceratitic sutures; red rhombuses: ammonitic sutures) (N=37)

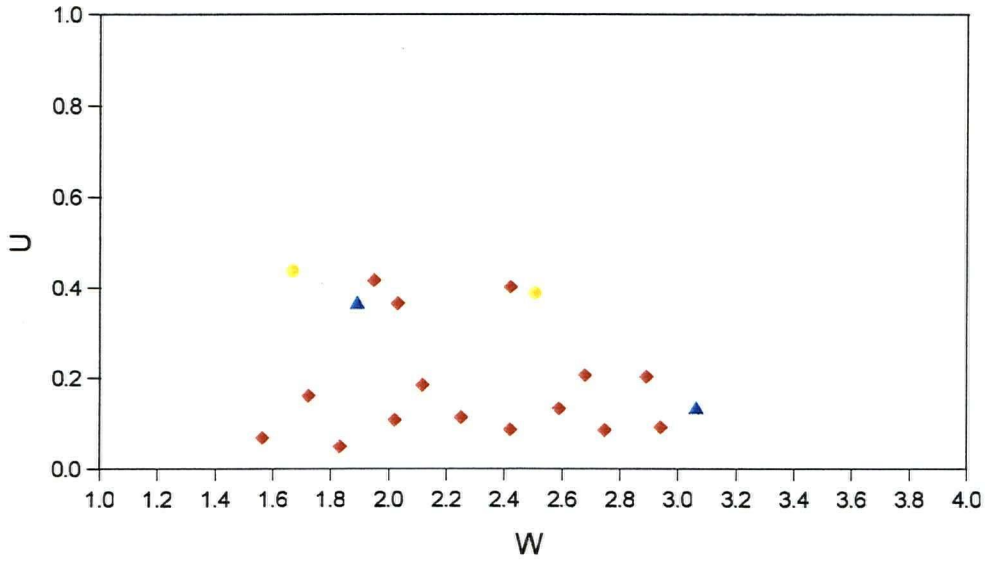

Figure 6-4 Carnian Stage Tropitaceae ammonoids W and U data (Yellow circles: goniatitic sutures; green triangles: ceratitic sutures; red rhombuses: ammonitic sutures) (N=19)

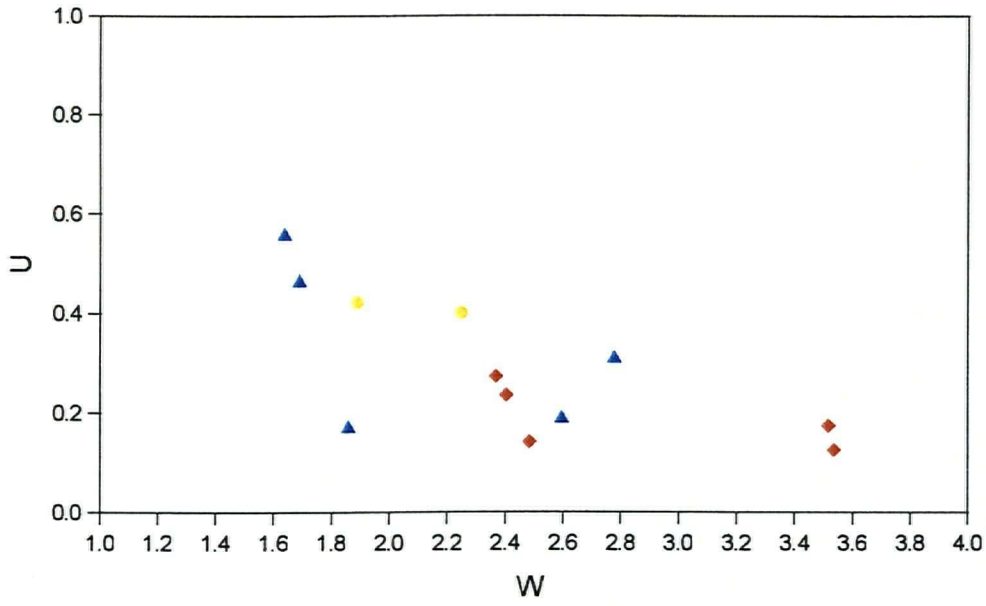

Figure 6-5 Carnian Stage Clydonitaceae ammonoids W and U data (Yellow circles: goniatitic sutures; green triangles: ceratitic sutures; red rhombuses: ammonitic sutures) (N=12)

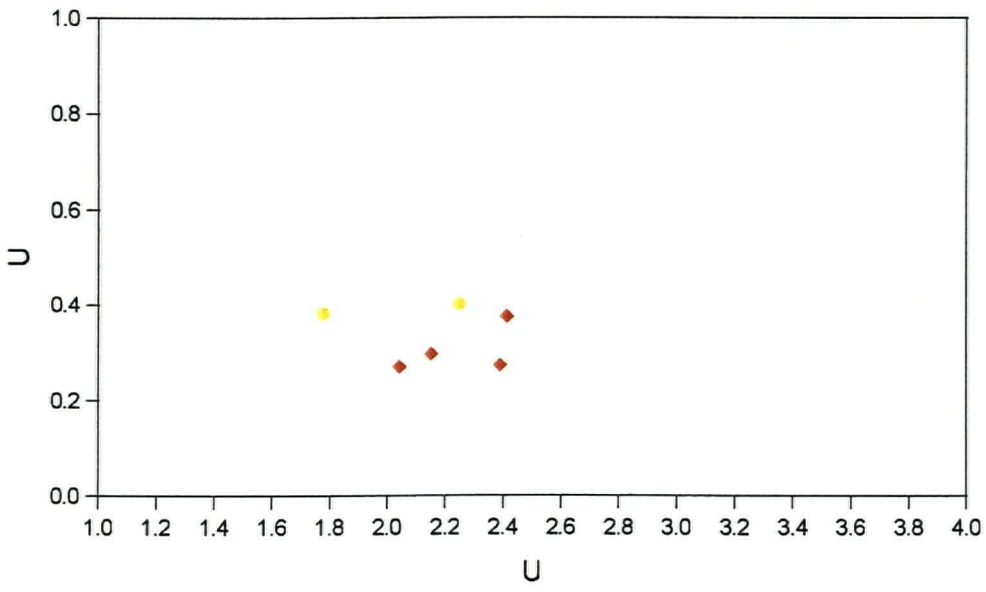

Figure 6-6 Carnian Stage Ceratitaceae, Choristoceratacera, Phylloceratacea ammonoids W and U data (Yellow circles: goniatitic sutures; green triangles: ceratitic sutures; red rhombuses: ammonitic sutures) (N=6)

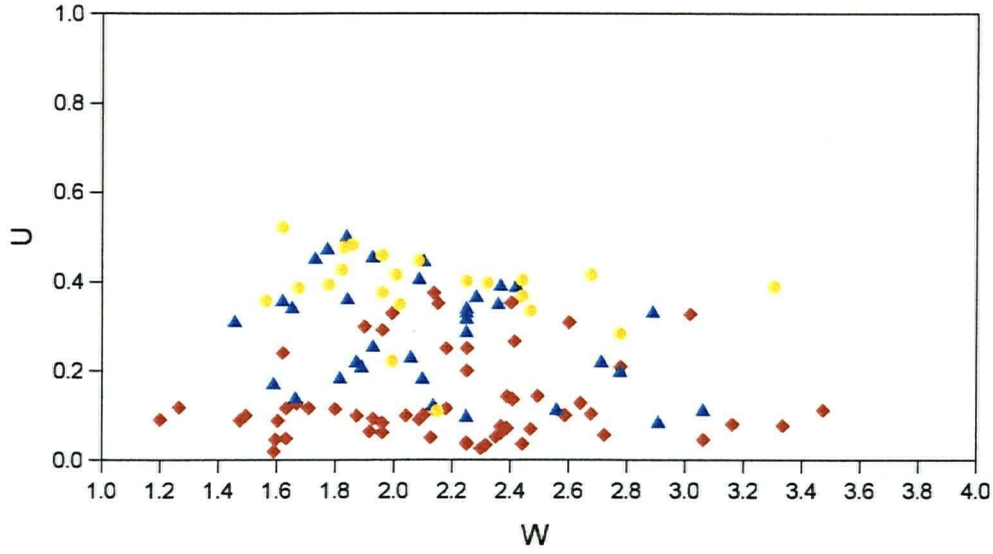

Figure 6-7 Norian Stage ammonoids W and U data (Yellow circles: goniatitic sutures; green triangles: ceratitic sutures; red rhombuses: ammonitic sutures) (N=113)

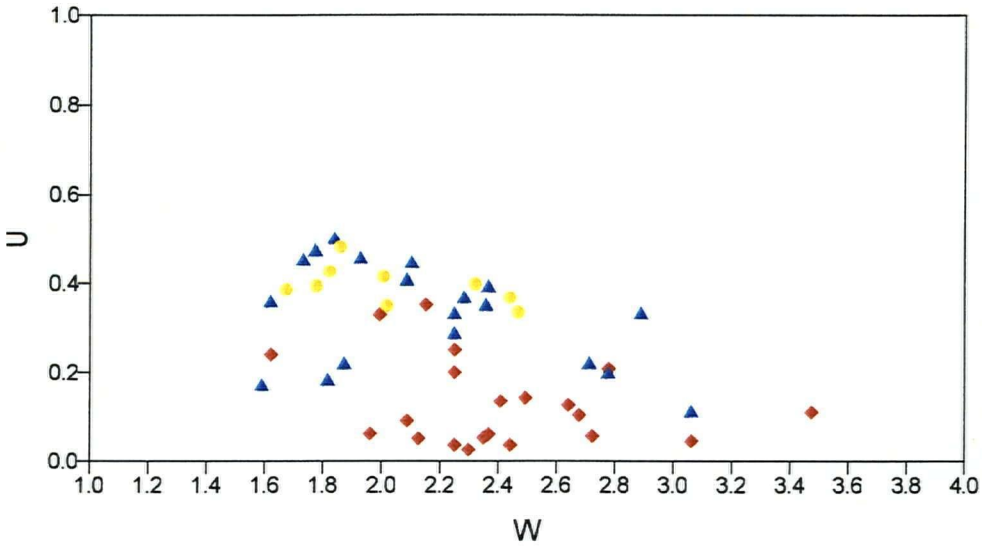

Figure 6-8 Norian Stage Nathoristitaceae ammonoids W and U data (Yellow circles: goniatitic sutures; green triangles: ceratitic sutures; red rhombuses: ammonitic sutures) (N=49)

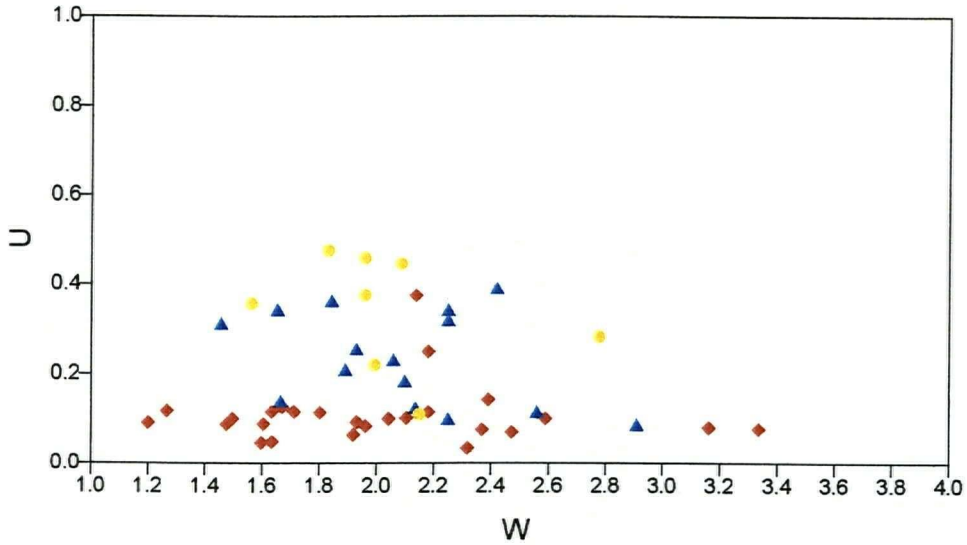

Figure 6-9 Norian Stage Tropitaceae ammonoids W and U data (Yellow circles: goniatitic sutures; green triangles: ceratitic sutures; red rhombuses: ammonitic sutures) (N=49)

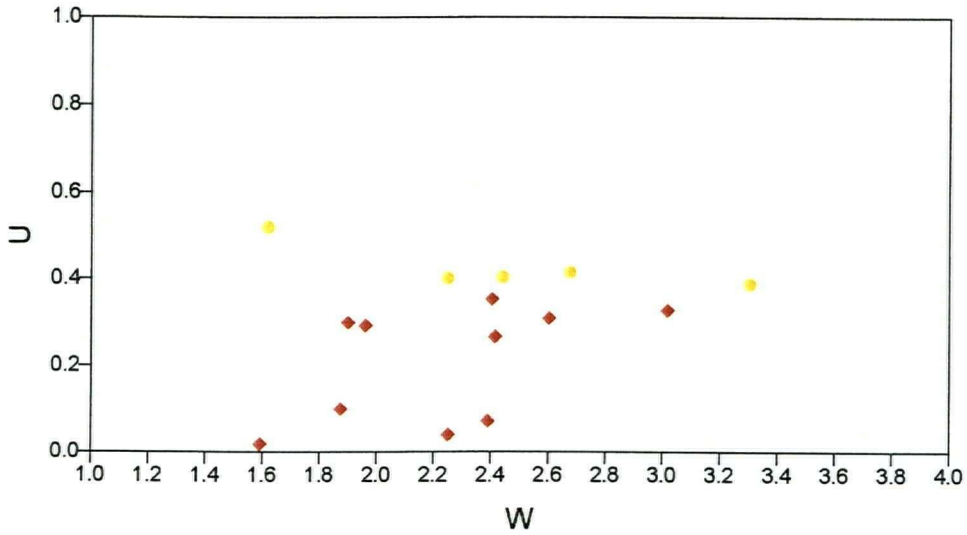

Figure 6-10 Norian Stage Ussuritaceae, Megaphyllitaceae, Pinacocerataceae, Choristoceratacear ammonoids W and U data (Yellow circles: goniatitic sutures; green triangles: ceratitic sutures; red rhombuses: ammonitic sutures) (N=15)

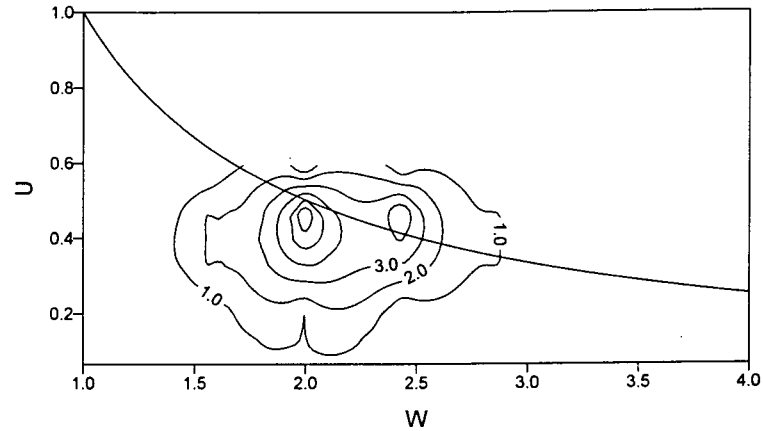

Figure 6-11 Contoured W-U density diagram for Carnian and Norian ammonoids having goniatitic sutures (N=28)

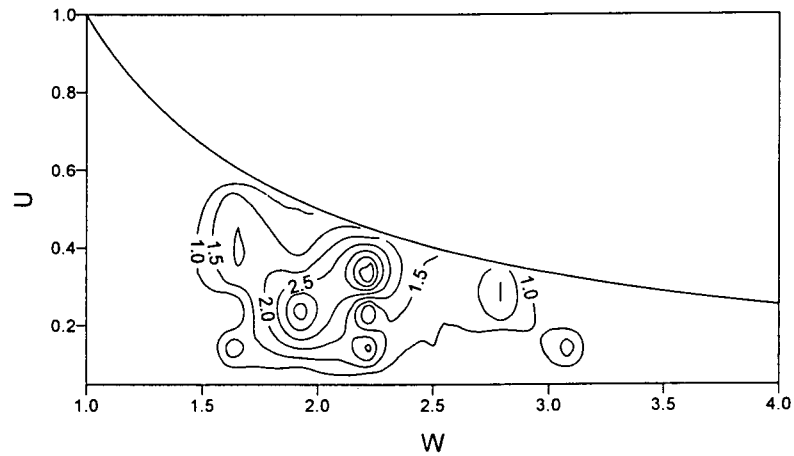

Figure 6-12 Contoured W-U density diagram for Carnian and Norian ammonoids having ceratitic sutures (N=41)

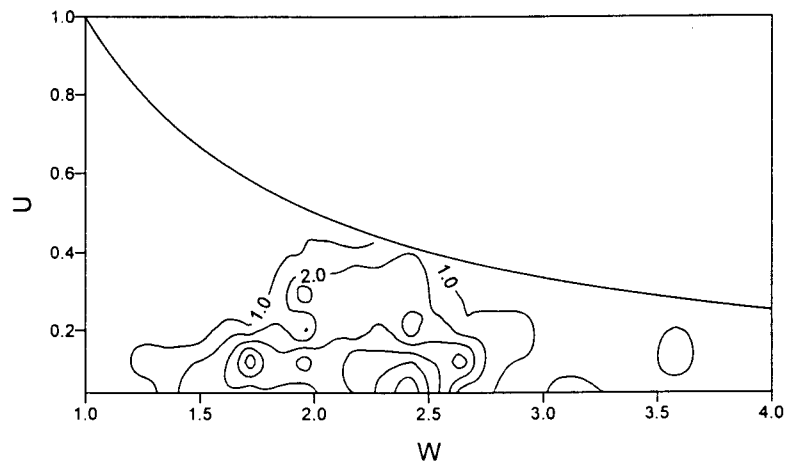

Figure 6-13 Contoured W-U density diagram for Carnian and Norian ammonoids having ammonitic sutures (N=81)

6.4 Discussion

The above figures show that the distribution of the sutures on the W-U geometric maps follows certain rules. The distribution of different sutures is correlated with U values while W values do not have much influence. The ammonitic sutures, which have the most complex structure, are distributed across the low U values region, while the simplest goniatitic sutures are in high U value areas. The ceratitic sutures are distributed between them. This indicates that, in the Late Triassic, the ammonoid suture type is affected by the extent of the shell's volution. Involute shells tend to have complex ammonitic sutures, while evolute shells tend to have simple goniatic sutures.

As we have discussed in Chapter 3 that the correlation between U and WWWH is positive, i.e., high U value shells tend to have depressed whorls (large WWWH values) while low U value shells tend to have compressed whorls (small WWWH values). We can infer that, for Carnian and Norian ammonoids, rounded whorl shells have relatively strong resistant to water pressure, so this type of shells does not need complex sutures to strengthen shells. While narrow whorled shells are weak for pressure, so the ammonitic suture can reinforce the shells to resist the water pressure.

However, Early Jurassic ammonoids only have ammonitic suture lines but their geometry distributes at high U regions (as discussed in Chapter 2). Unlike those in the Upper Triassic, the distribution of sutures and shell geometry across the T-J boundary do not correlate. This counter intuitive suture-geometry distribution pattern poses a question to be resolved.

Chapter 7 Conclusions

This thesis mainly presents the research results on ammonoid morphological analysis of Late Triassic Carnian Stage through Middle Jurassic Bajocian Stage in order to establish the morphospace spectrum through T/J boundary. The major conclusions reached are as follows:

1. By using Raup's approach of ammonoid morphology modeling, Upper Triassic and Lower-Middle Jurassic ammonoid data are selected to set up the spectrum of geometries, which display that the ammonoid morphological evolution through the end-Triassic extinction is a remoulding process. Based on W-U density geometry patterns and the existence of heteromorph ammonoid groups, three intervals are recognized, namely the pre-extinction, post-extinction, and recovery intervals corresponding to the Late Triassic, Early Jurassic, and Middle Jurassic.

2. Knowledge of morphological covariation between whorl shape and shell geometry is important in the study of the relationship between shell form and shell function. There exists a positive correlation between whorl shape (WWWH) and whorl expansion (W), and a negative correlation between WWWH and umbilical ratio (U).

3. The hydromechanical efficiency of ammonoids from Upper Triassic Carnian Stage through Middle Jurassic Bajocian Stage is discussed in the thesis due to its importance in evaluating ammonoid paleobiology. The ammonoid mobility and the interrelation between morphology and hydrodynamic through these stages are explored. The correlation between W-U density geometries and the low C_D point positions indicates that the Later Triassic and Middle Jurassic ammonoids have broad distribution across W-

U morphospace and relatively low hydromechanical efficiency. Early Jurassic ammonoids have better hydromechanical efficiency and linear W-U geometric patterns.

4. The plot of ammonoid accumulated morphological range diversity index (MRDI) for nine selected geometry and ornamentation characters shows there are two MRDI declines, one in the Hettangian Stage and a second in the Aalenian Stage, times when some important ammonoid groups disappeared as the result of extinction.

5. The correlation between Upper Triassic ammonoid suture types and shell geometry is another issue discussed in the thesis. Involute Upper Triassic shells tend to have complex sutures, whereas evolute shells tend to have simple sutures. However, in Early Jurassic ammonoids only have complex suture lines but their geometry distribute at high U areas (involute forms). These different suture-geometry patterns for Upper Triassic and Lower Jurassic ammonoids have not yet been explained.

References

Arkell, W.J., Furnish, W. M., Kummel, B., Miller, A. K., Moore, R. C., Schindewolf, O. H., Sylvester-Bradler, P. C., and Wright C. W. 1957. Treatise on Invertebrate Paleontology (Part L). Geological Society of America and University of Kansas Press.

Benton, M. J. 1986. More than one event in the late Triassic mass extinction. Nature, **321**: 857-861.

Chamberlain, J. A. 1971. Shell morphology and the dynamics of streamlining in ectocochliate cephalopods (abstr.). Geol. Soc. Am. Abstr. with Prog. **3**:523-524.

Chamberlain, J. A. 1973. Phyletic improvements in hydromechanical design and swimming ability in fossil nautiloids (abstr.). Geol. Soc. Am. Abstr. with Prog. **5**:571-572.

Chamberlain, J. A. 1976. Flow pattern and drag coefficients of cephalopod shells. Palaeontology, 19(3): 539-563.

Chamberlain, J.A. 1980. Hydromechanical design of fossil cephalopods. In: House, M.R. and Senior, J.R. eds. The Ammonoidae. Systematics Association Special Volume **18**: 289-336.

Dommergues, J.-L. and Meister, C. 1987. succession des faunes d'ammonites au langenegggrat (préalpes médianes, région de thoune, suisse): une série de référence dans le sinémurien supérieur. Geobios, n° 20, fasc. **3**: 313-335.

Dommergues, J.-L. and Meister, C. 1989. succession des faunes d'ammonites du sinémurien supérieur dans le chablais méridional et les klippes de savoie (préalpes médianes, haute-savoie, france). Geobios, n° 22, fasc. **4**: 455-483.

Dommergues, J.-L., Laurin, B., and Meister, C. 1996. Evolution of ammonoid mophospace during the Early jurassic radiation. Paleobiology, **22(2)**: 219-240.

Dommergues, J.-L., Laurin, B., and Meister, C. 2001. The recovery and radiation of Early

Jurassic ammonoids: mophologic versus palaeobiogeographical patterns. Palaeogeography, Palaeoclimatology, Palaeoecology, **165**: 195-213.

Donovan, D.T. 1998. A new ammonite genus from the Lower Jurassic (Upper Sinemurian) of Dorset, England. Palaeontology, **41(5)**: 993-999.

Foote, M. 1991. Morphologic patterns of diversification: examples from trilobites. Paleontology, **34(2)**: 461-485.

Gert Bloos, S. 1999. *Neophyllites* (Ammonoidea, Psiloceratidae) in the earliest Jurassic of South Germany. N. Jb. Geol. Paläont. Abh., **211(1/2)**: 7-29.

Gradstein, F. M., Agterberg, F. P., Ogg, J. G., Hardenbol, J., van Veen, P., Thierry, J., and Huang, Z. 1994. A Mesozoic time scale: Joural of Geophysical Research. **99**: 24051-24074.

Guex, J. 1987. Sur la phylogenèse des ammonites du Lias inférieur. Bull. Soc. Vaud. Sc. Nat. **78.4**: 455-469.

Guex, J., Taylor, D., Rakus, M., and Bucher, H., 1998. Deux nouveaux genres et quatre nouvelles espèces d'ammonites (Cephalopoda) du Lias inférieur. Bull. Soc. Vaud. Sc. Nat. **86.1:** 73-85.

Hall, R. L. and Westermann, E. G. 1980. Lower Bajocian (Jurassic) Cephalopod faunas from western Canada and proposed assemblage zones for the Lower Bajocian of North America. Palaeontographica Americana, **9(52)**: 1-93.

Haq, B. U., Hardenbol, J., and Vail, P. R. 1988. Mesozoic and Cenozoic chronostratigraphy and cycles of sea level change. Society of Economic Paleontologists and Mineralogists Special Publication. **42**: 71-108.

Harland, W. B., Armstrong, R. L., Cox, A. V., Craig, L. E., Smith, A. G., Smith, D. G. 1989. A geologic time scale 1989. Cambridge University Press.

Kullmann, J., Korn, D., Kullmann, P. S. and Petersen, M. S. 1991. The status of GONIAT, a

data-base for Paleozoic ammonoids. First Canadian Paleontology Conference, Vancouver. P.48.

Lehmann, U. 1981. The ammonites-Their life and their world. Cambridge University Press.

Liang, B. 1994. A lower Jurassic ammonite image database and its application.

Liang, B. and Smith, P. L. 1997. The Jurassic Ammonite Image Database 'Ammon". Palaeontology, **40(1)**: 99-112.

Ludwigsburg, G. D. 1977. The Braunjura (Brown Jurassic) in Southwest Germany. Stuttgarter Bertr. Naturk., Ser. B, Nr. **25:** 1-41.

Odin, G. S. 1994. Geological time scale: Comptes Rendus de l'Académie des Sciences, Paris. **318**: 59-71.

Okamoto, T. 1988. Analysis of heteromorph ammonoids by differential geometry. Palaeontology, **31(1)**: 35-52.

Pálfy, J., Mortensen, J. K., Carter, E. S., Smith, P. L., Friedman, R. M., and Tipper, H. W. 2000a. Timing the end-Triassic mass extinction: First on land, then in the sea? Geology, **28(1)**: 39-42.

Pálfy, J., Mortensen, J. K., Smith, P. L., Friedman, R. M., McNicoll, V., and Villeneuve, M. 2000b. New U-Pb zircon ages integrted with ammonite biochronology from the Jurassic of the Canadian Cordillera. Can. J. Earth Sci. **37**: 549-567.

Rakús, M. 1993. Late Triassic and Early Jurassic Phylloceratids from the Salzkammergut (Northern Calcareous Alps). Jahrbuch der Beologischen Bondesanstalt Wien, **136(4)**: 933-963.

Raup, D. M. 1966. Geometric Analysis of Shell Coiling: General Problems. Journal of Paleontology, **40(5)**: 1178-1190.

Raup, D. M. 1967. Geometric Analysis of Shell Coiling: Coiling in Ammonoids. Journal of

Paleontology, **41(1)**: 43-65.

Raup, D. M. and Sepkoski, Jr., J. J. 1982. Mass extinction in the marine fossil record. Science, **215**: 1501-1502.

Schlegelmilch, R. 1985. Die Ammoniten des süddeutschen Doggers. Gustav Fischer Verlag, Stuttgart, New York.

Smith, P. L. 1986. The implications of data base management systems to paleontology: A discussion of Jurassic ammonoid data. Journal of Paleontology, **60(2)**: 327-340.

Smith, P. L. and Tipper, H. W. 1996. Pliensbachian (Lower jurassic) Ammonites of the Queen Charlotte Islands, British Columbia. Bulletins of American Paleontology, **108(348)**: 1-122.

Smith, P. L. and Tipper, H. W. 2000. The schlotheimiid succession across the Hettangian-Sinemurian boundary (Lower Jurassic), Taseko Lakes map area, British Columbia, Canada. Revue Paléobiol., Genève (2000) Vol. spéc. **8:** 1-12.

Stuttgart, V. G. D. 1978. Die heteromorphen Ammoniten des Dogger. Stuttgarter Beitr. Naturk., Ser. B, Nr. 33: 1-97.

Tozer, E.T. 1981. Triassic Ammonoidea: classification, evolution and relationship with Permian and Jurassic forms. In: House, M.R. and Senior, J.R. eds. The Ammonoidae. Systematics Association Special Volume 18: 65-100.

Tozer, E. T. 1994. Canadian Triassic Ammonoid Faunas. Geological Survey of Canada Bulletin 467. 1-663.

Westermann, G. E. G. 1966. Covariation and taxonomy of the Jurassic ammonite *Sonninia adicra* (Waagen). N. Jb. Geol. Paläont. Abh., **124(3)**: 289-312.

Wiedmann, J. 1973. Upper Triassic Heteromorph Ammonites. In: Hallam, A. eds. Atlas of Palaeobiogeography. Elsevier Scientific publishing Company.